

Electronic Supplementary Information

Facile Synthesis of Functionalized Urea, Imidazolium Salt, Azide and Triazole from 2-Amino-5,7-Dimethyl-1,8-Naphthyridine Scaffold and their Utilization in Fluoride ion Sensing.

Mandeep K. Chahal, Tawseef Ahmad Dar and M.Sankar*

Department of Chemistry, Indian Institute of Technology Roorkee, Roorkee-247667, India

Table of Contents

	Page No
Figure S1. ^1H NMR spectrum of 1a in DMSO- d_6 at 298K.	4
Figure S2. ^{13}C NMR spectrum of 1a in DMSO- d_6 at 298K.	4
Figure S3. HRMS (ESI+) mass spectrum of 1a in CH ₃ CN.	5
Figure S4. FT-IR spectrum of 1a in KBr pellet.	5
Figure S5. ^1H NMR spectrum of 1b in DMSO- d_6 at 298K.	6
Figure S6. ^{13}C NMR spectrum of 1b in DMSO- d_6 at 298K.	6
Figure S7. HRMS (ESI+) mass spectrum of 1b in CH ₃ CN.	7
Figure S8. FT-IR spectrum of 1b in KBr pellet.	7
Figure S9. ^1H NMR spectrum of nap-Br in CDCl ₃ at 298 K.	8
Figure S10. HRMS (ESI+) mass spectrum of nap-Br in CH ₃ CN.	8
Figure S11. FT-IR spectrum of nap-Br in KBr pellet.	9
Figure S12. ^1H NMR spectrum of 2 in DMSO- d_6 at 298K.	9
Figure S13. ^{13}C NMR spectrum of 2 in DMSO- d_6 at 298K.	10
Figure S14. HRMS (ESI+) mass spectrum of 2 in CH ₃ CN.	10
Figure S15. FT-IR spectrum of 2 in KBr pellet.	11
Figure S16. ^1H NMR spectrum of 3 in DMSO- d_6 at 298 K.	11
Figure S17. ^{13}C NMR spectrum of 3 in DMSO- d_6 at 298 K.	12
Figure S18. HRMS (ESI+) mass spectrum of 3 in CH ₃ CN.	12
Figure S19. FT-IR spectrum of 3 in KBr pellet.	13
Figure S20. ^1H NMR spectrum of 4 in DMSO- d_6 at 298K.	13
Figure S21. ^{13}C NMR spectrum of 4 in DMSO- d_6 at 298K.	14
Figure S22. FT-IR spectrum of 4 in KBr pellet.	14
Figure S23. Benesi–Hildebrand plot for the titration of 1a versus F ⁻ ions showing a 1:1 binding stoichiometry.	15
Figure S24. Change in UV-Vis spectrum for receptor 1a at r. t. (4×10^{-5} M) in DMSO upon the addition of 0 to 4×10^{-3} M of cyanide ions.	15
Figure S25. Change in UV-Vis spectrum for receptor 1b at r. t. (4×10^{-5} M) in DMSO upon the addition of excess of fluoride ions.	16
Figure S26. Change in UV-Vis spectrum for receptor 2 at r. t. (12×10^{-5} M) in DMSO upon the addition of 0 - 7.69×10^{-4} M (6.4 equiv.) of fluoride ions.	16
Figure S27. Job's plot for fluoride- 2 interactions. The total ([F ⁻] + [2]) = 6.45×10^{-5} M.	17
Figure S28. Benesi–Hildebrand plots for the titration of 2 versus F ⁻ ions showing a 1:1 binding	17

stoichiometry.	
Figure S29. Change in UV-Vis spectrum for receptor 2 at r. t. (12×10^{-5} M) in DMSO upon the addition of 0 to 13.2×10^{-4} M (11 equiv.) of cyanide ions.	18
Figure S30. Absorption spectra of compound 1a (4×10^{-5} M) upon addition of tetrabutylammonium F ⁻ , I ⁻ , Br ⁻ , OAc ⁻ , Cl ⁻ , H ₂ PO ₄ ⁻ , ClO ₄ ⁻ , HSO ₄ ⁻ , NO ₃ ⁻ , PF ₆ ⁻ and CN ⁻ (1.2×10^{-3} M) in DMSO.	18
Figure S31. Absorption spectra of compound 2 (12×10^{-5} M) upon addition of tetrabutylammonium F ⁻ , I ⁻ , Br ⁻ , OAc ⁻ , Cl ⁻ , H ₂ PO ₄ ⁻ , ClO ₄ ⁻ , HSO ₄ ⁻ , NO ₃ ⁻ , PF ₆ ⁻ and CN ⁻ (8 equiv.) in DMSO.	19
Figure S32. Selectivity of anions at wavelength 462 nm in a solution having 1a + anions (blue bar) and 1a + anions + F ⁻ (red bar) observed using UV-Vis spectral studies. (a) all X ⁻ (b) Br ⁻ (c) HSO ₄ ⁻ (d) I ⁻ (e) BH ₄ ⁻ (f) ClO ₄ ⁻ (g) CH ₃ COO ⁻ (h) PF ₆ ⁻ (i) H ₂ PO ₄ ⁻ (j) NO ₃ ⁻ (k) Cl ⁻ (l) CN ⁻ .	19
Figure S33. Selectivity of anions at wavelength 360 nm in a solution having 2 + anions (blue bar) and 2 + anions + F ⁻ (red bar) observed using UV-Vis spectral studies. (a) all X ⁻ (b) Br ⁻ (c) HSO ₄ ⁻ (d) I ⁻ (e) BH ₄ ⁻ (f) ClO ₄ ⁻ (g) CH ₃ COO ⁻ (h) PF ₆ ⁻ (i) H ₂ PO ₄ ⁻ (j) NO ₃ ⁻ (k) Cl ⁻ (l) CN ⁻ .	20
Figure S34. Fluorescence changes of 1a upon the addition of tetrabutylammonium fluoride in DMSO at r.t.	20
Figure S35. Fluorescence changes of 1a upon the addition of different anions (a) CH ₃ COO ⁻ (b) Br ⁻ (c) Cl ⁻ and (d) ClO ₄ ⁻ in DMSO at 298 K.	21
Figure S36. Fluorescence changes of 1a upon the addition of different anions (a) CN ⁻ (b) H ₂ PO ₄ ⁻ (c) HSO ₄ ⁻ and (d) I ⁻ in DMSO at 298 K.	21
Figure S37. Fluorescence changes of 1a upon addition of (a) NO ₃ ⁻ and (b) PF ₆ ⁻ in DMSO at 298 K.	22
Figure S38. Fluorescence changes for receptor 2 at r. t. (1×10^{-5} M) in DMSO upon the addition of 0 – 6.4×10^{-5} M (6.4 equiv.) of fluoride ions.	22
Figure S39. Fluorescence changes of 2 upon addition of different anions (a) ClO ₄ ⁻ (b) CH ₃ COO ⁻ (c) Br ⁻ and (d) Cl ⁻ in DMSO at 298 K.	23
Figure S40. Fluorescence changes of 2 upon addition of different anions (a) CN ⁻ (b) H ₂ PO ₄ ⁻ (c) HSO ₄ ⁻ and (d) I ⁻ in DMSO at 298 K.	23
Figure S41. Fluorescence changes of 2 upon the addition of (a) NO ₃ ⁻ and (b) PF ₆ ⁻ in DMSO at 298 K.	24
Figure S42. ¹ H-NMR Titration of a 5×10^{-3} M solution of 2 in DMSO-d ₆ with increasing concentration of F ⁻ ions.	24
Figure S43. DFT optimized structures of 1a and 1a •F ⁻ in DMSO.	25
Figure S44. HOMO-LUMO energy gaps for 1a and 1a •F ⁻ complex in DMSO.	25
Figure S45. (a) DFT-optimized structures of 2 along with its fluoride complex in Gas phase calculated at B3LYP/6-31+G(d,p) level of theory. (b) DFT optimized structures of 2 in (A) gas phase and in (B) DMSO.	26
Figure S46. HOMO-LUMO energy gaps for 2 and 2 •F ⁻ complex.	26
Figure S47. Absorption spectra of 2 , 2 ⁻ , and (2 •F ⁻) calculated by TD-DFT calculations.	27
Figure S48. Colorimetric response of 1a for reversibility and reusability tests with OH ⁻ ions (top) and their corresponding UV-Vis spectral changes in DMSO at 298 K (bottom).	27
Figure S49. UV-Vis spectral response of 2 for reversibility and reusability tests with F ⁻ ions in DMSO at 298 K.	28
Figure S50. UV-Vis spectral response of 2 for reversibility and reusability tests with OH ⁻ ions in DMSO at 298 K.	28

Figure S51. Absorbance of 1a in DMSO, normalized between the minimum absorbance found at zero equiv of F ⁻ and the maximum absorbance found at 13 eq. of F ⁻ .	29
Figure S52. Absorbance of 2 in DMSO, normalized between the minimum absorbance found at zero equiv of F ⁻ and the maximum absorbance at 3 eq. of F ⁻ .	29
Figure S53. H/D exchange confirmed that -CH ₂ protons are less acidic as the peak at 5.37 ppm did not disappear on adding D ₂ O.	30
Table S1: Energy of the optimized molecules in DMSO and gaseous phases.	30
Table S2: Cartesian coordinates for 1a in DMSO.	30
Table S3: Cartesian coordinates for 1a in gas phase.	32
Table S4: Cartesian coordinates for 1a•F⁻ in DMSO.	33
Table S5: Cartesian coordinates for 1a•F⁻ in gas phase.	34
Table S6: Cartesian coordinates for 2 in DMSO.	36
Table S7: Cartesian coordinates for 2 in gas phase.	37
References	38

Experimental Section

All reagents were purchased from Alfa Aesar, HiMedia and were used without further purification. DMSO (HPLC grade) was used to perform spectral studies. UV-Visible spectra were recorded on an Agilent Cary 100 spectrophotometer, using a pair of quartz cells of 10 mm path length. ¹H NMR spectra were recorded on a Bruker AVANCE 500 MHz spectrometer and JEOL ECX 400 MHz instruments in DMSO-*d*₆. The elemental analyses were performed on an Elementarvario EL III instrument. HRMS-ESI mass spectra were recorded on a BrukerDaltanics micro-TOF mass spectrometer using CH₃CN as solvent.

UV-Vis and ¹H NMR titrations

UV-Vis titrations were performed using a freshly prepared solution of receptors (**1a** and **2**) in DMSO. To this, aliquots of freshly prepared solutions (2 x 10⁻³ M) of tetrabutylammonium salts, TBAX where X = F⁻, I⁻, Br⁻, OAc⁻, Cl⁻, H₂PO₄⁻, ClO₄⁻, HSO₄⁻, NO₃⁻, PF₆⁻ and CN⁻ were added in DMSO. ¹H NMR titrations were also performed using freshly prepared solutions in deuterated solvents. The deprotonation and association constants as well as stoichiometry were calculated using Benesi-Hildebrand plots.

DFT calculations

All calculations were carried out using density functional theory(DFT)¹ with Becke's three-parameter hybrid exchange functional and the Lee-Yang-Parr correlation functional abbreviated as the B3LYP level of theory using the 6-31+G(d,p) basis set. Analytical frequency calculations were carried out for the geometry optimized structure to ensure the minima on the potential energy surface. The absorption wavelengths and oscillator strengths were calculated using time-dependent density-functional theory (TD-DFT).² NMR shielding tensors were computed with the Gauge-Independent Atomic Orbital (GIAO) method.³ Currently available functionals do not include a magnetic field dependence, so DFT methods do not provide systematically better NMR results than Hartree-Fock (HF).⁴ Therefore, the chemical shifts were calculated at the HF level with the 6-31+G(d,p) basis set at the B3LYP/6-31+G(d,p)-optimized geometries.

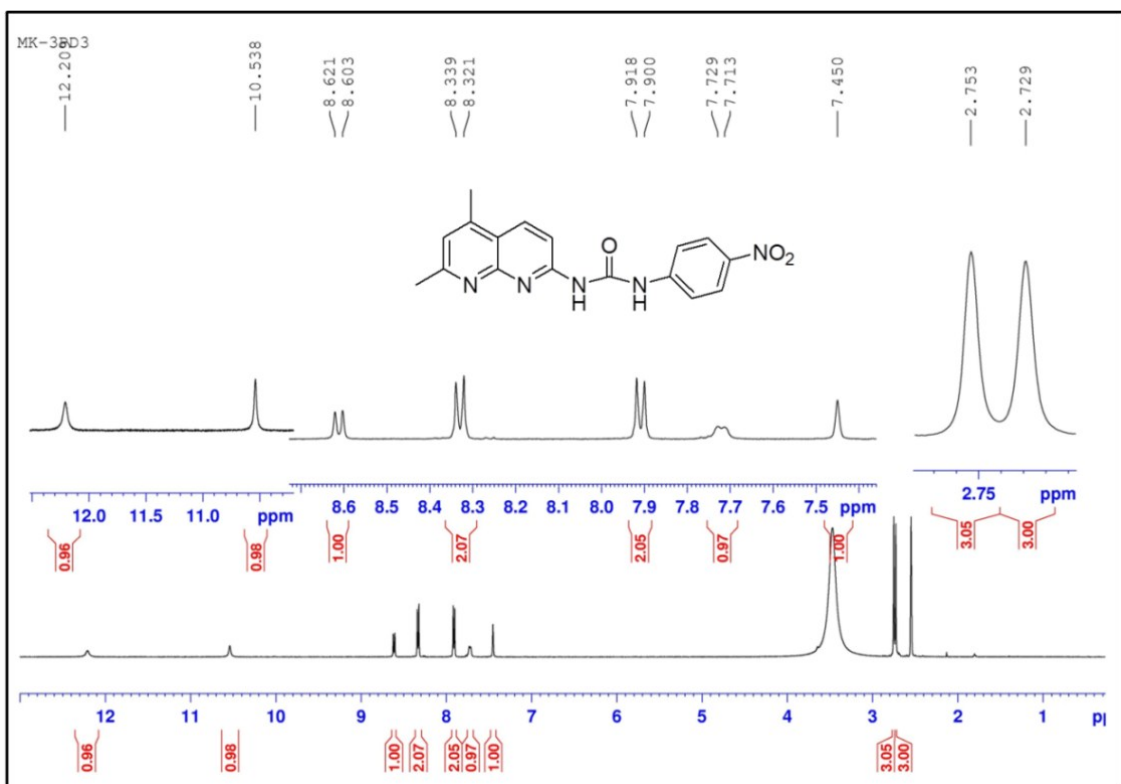


Figure S1. ^1H NMR spectrum of **1a** in $\text{DMSO}-d_6$ at 298K.

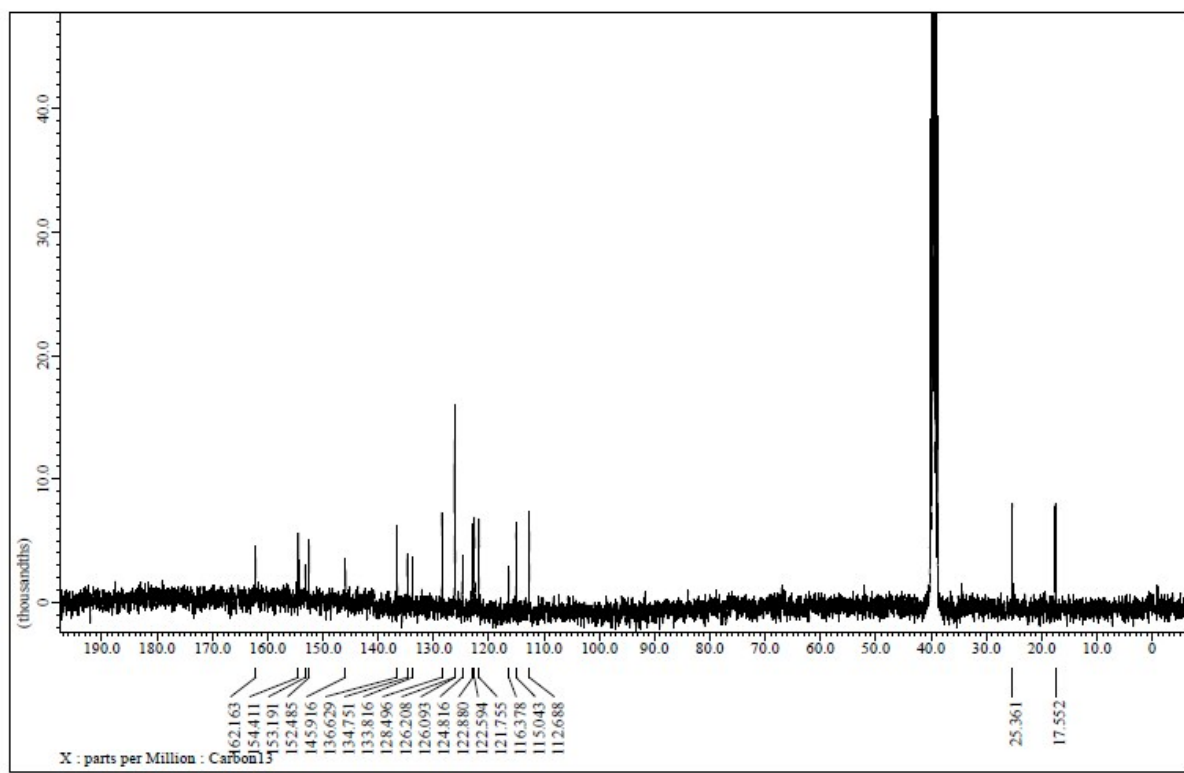


Figure S2. ^{13}C NMR spectrum of **1a** in $\text{DMSO}-d_6$ at 298K.

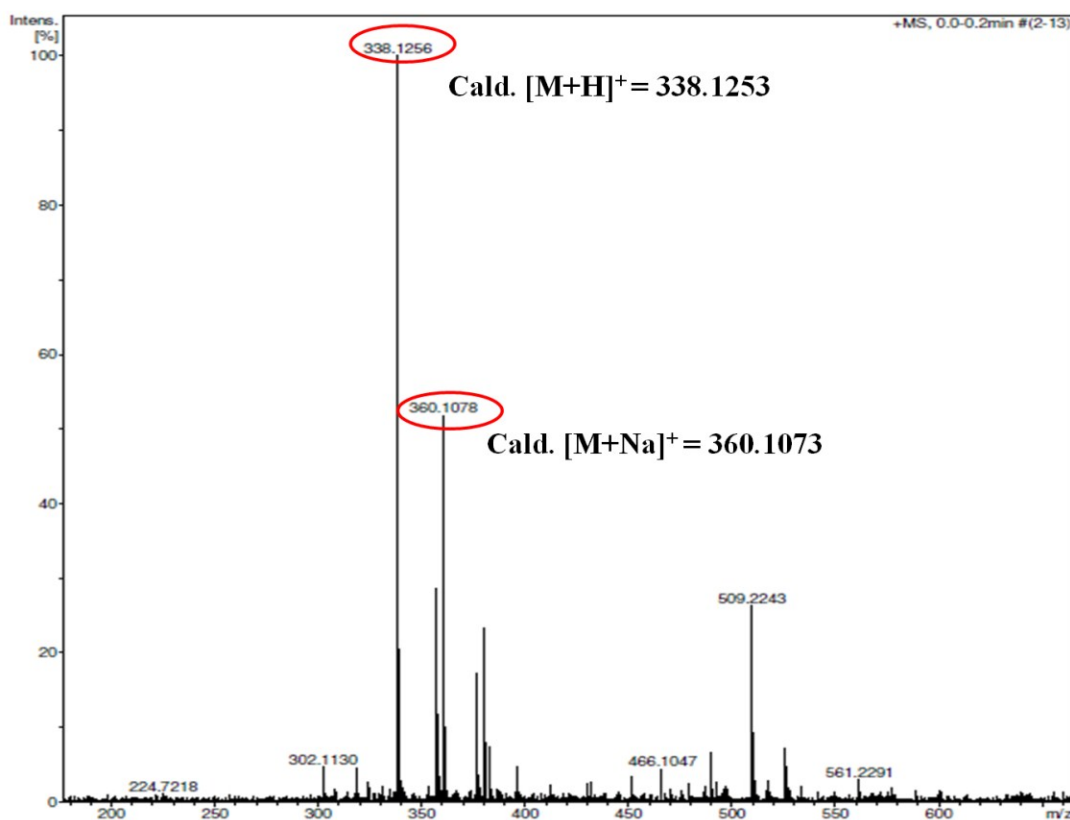


Figure S3. HRMS (ESI⁺) mass spectrum of **1a** in CH₃CN.

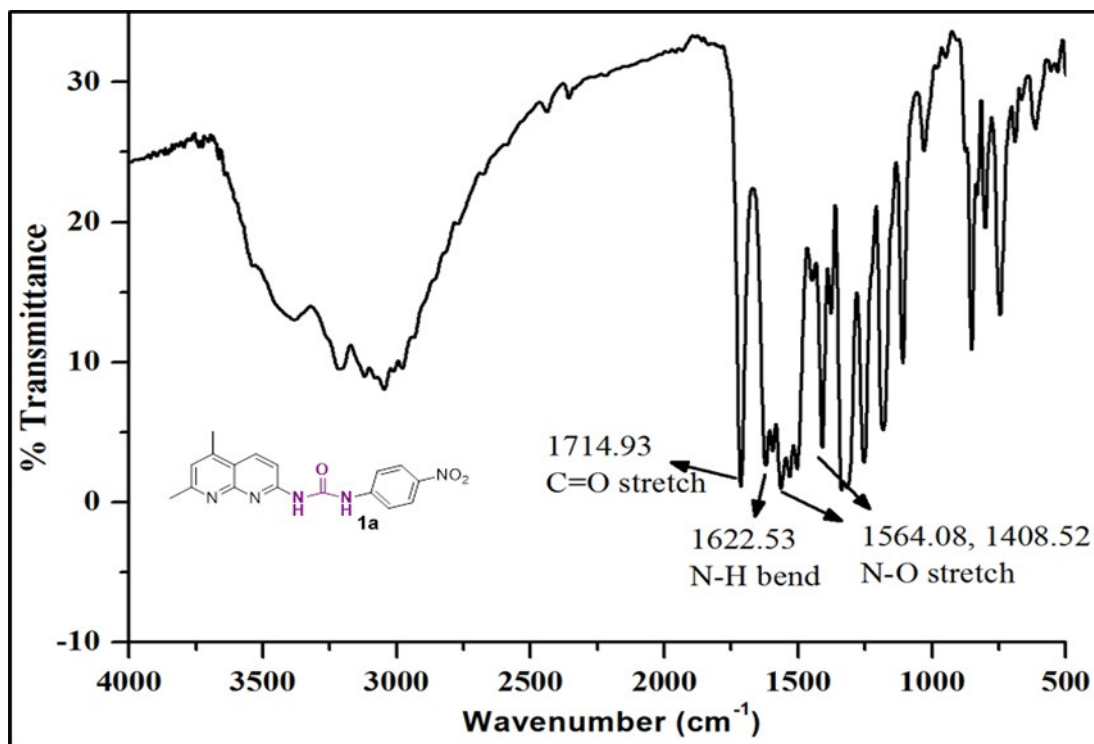


Figure S4. FT-IR spectrum of **1a** in KBr pellet.

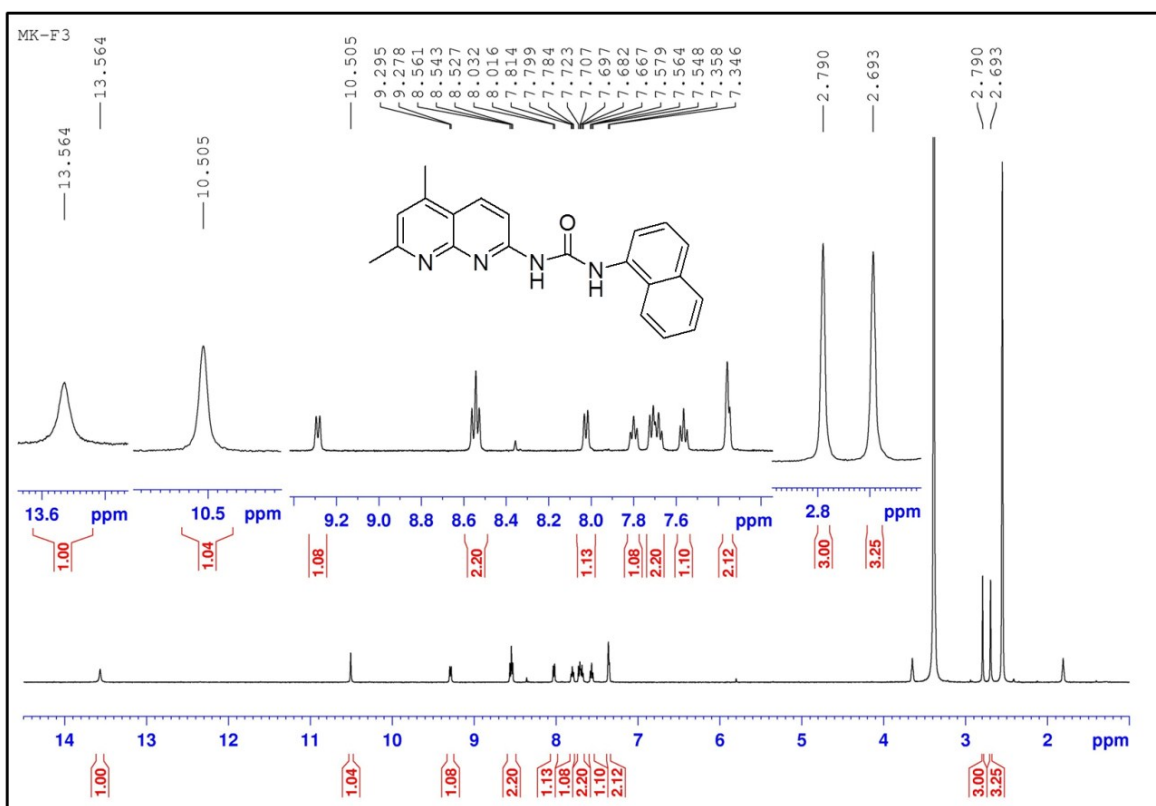


Figure S5. ^1H NMR spectrum of **1b** in $\text{DMSO}-d_6$ at 298K.

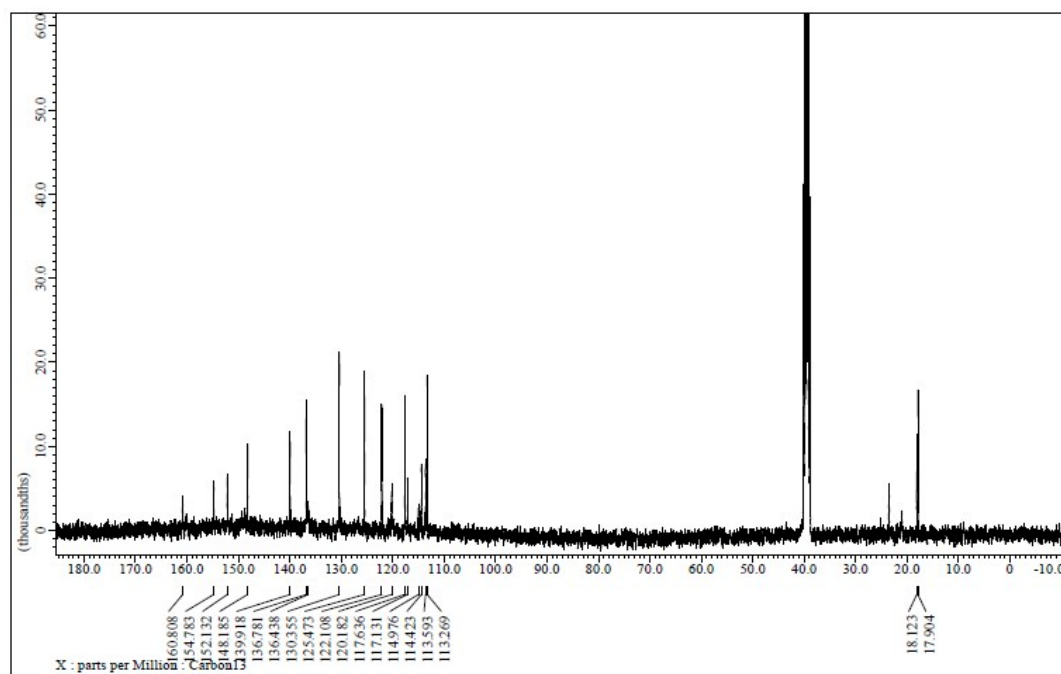


Figure S6. ^{13}C NMR spectrum of **1b** in $\text{DMSO}-d_6$ at 298K.

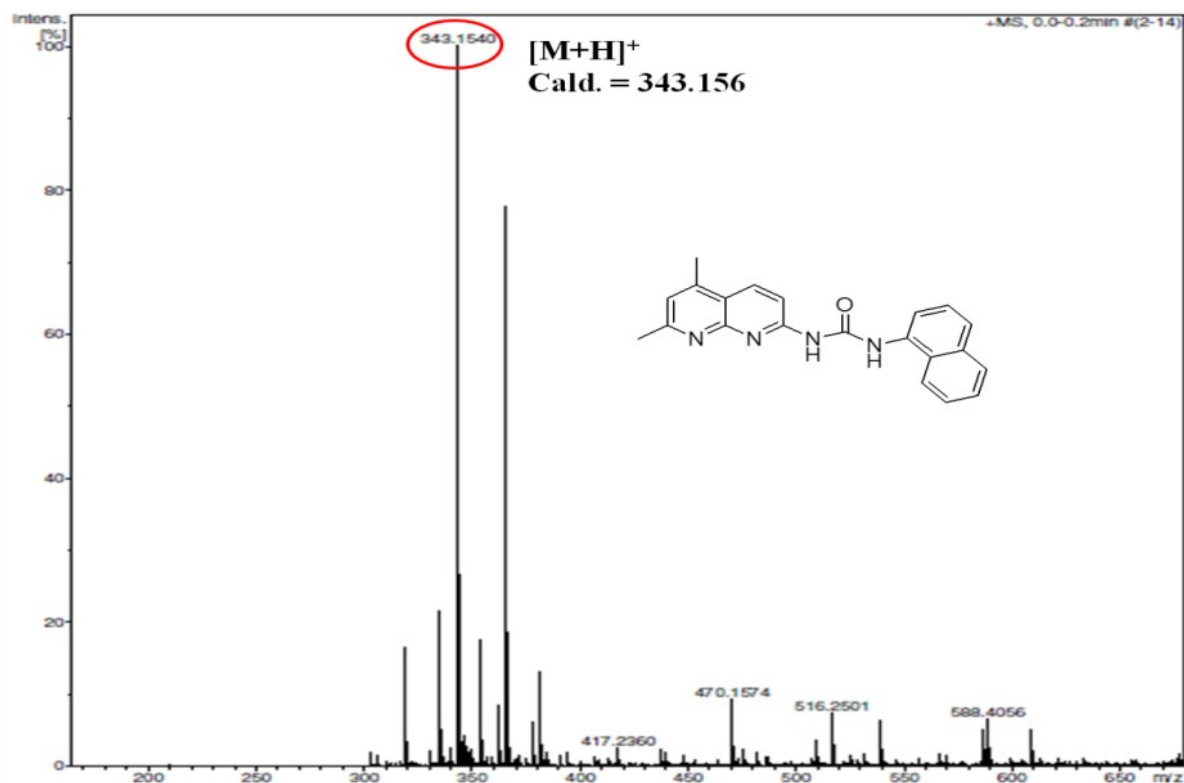


Figure S7. HRMS (ESI+) mass spectrum of **1b** in CH₃CN.

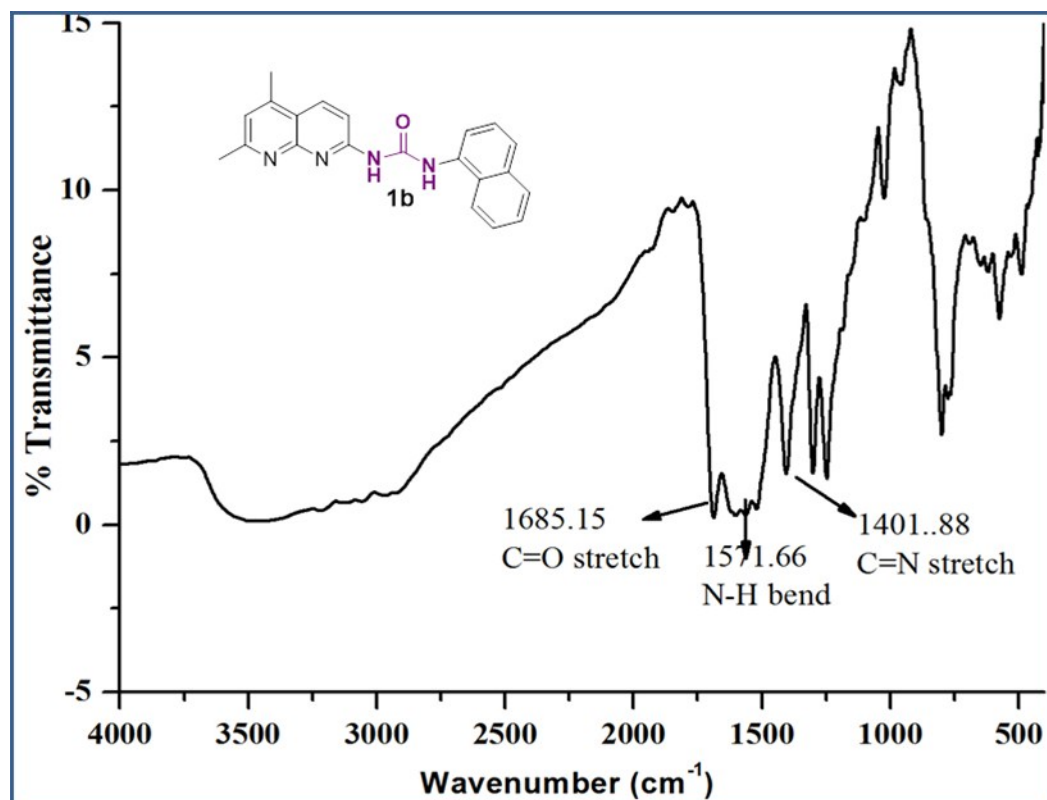


Figure S8. FT-IR spectrum of **1b** in KBr pellet.

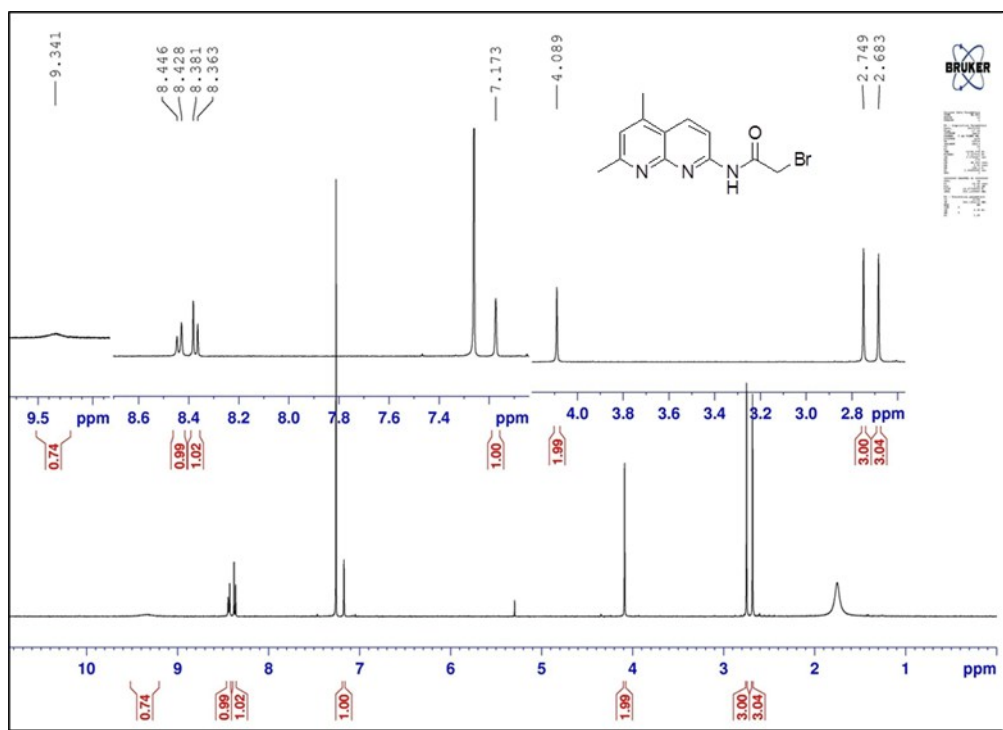


Figure S9. ^1H NMR spectrum of **nap-Br** in CDCl_3 at 298 K.

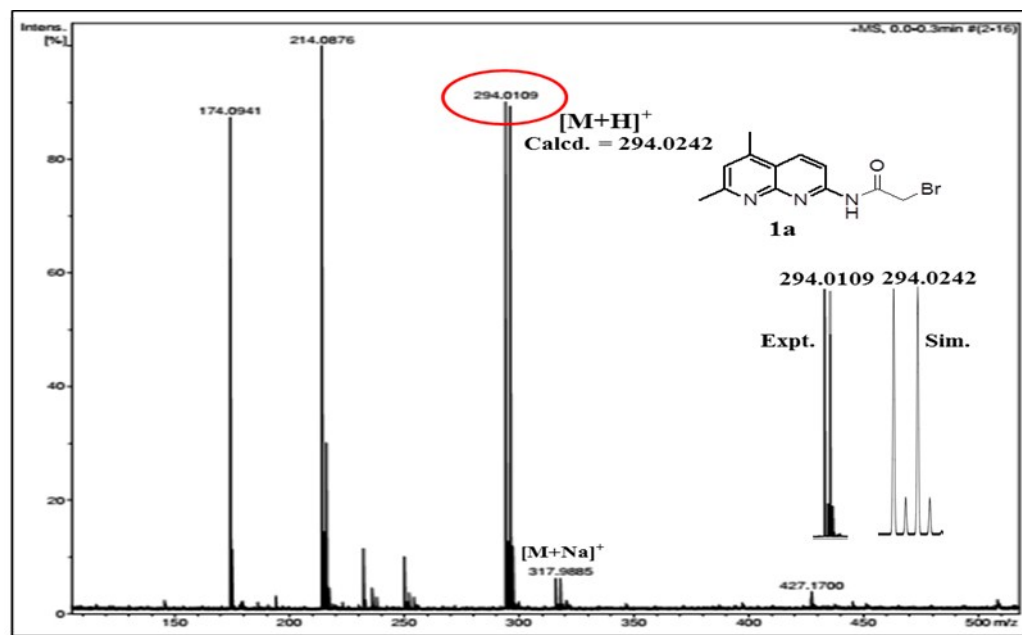


Figure S10. HRMS (ESI+) mass spectrum of nap-Br in CH₃CN.

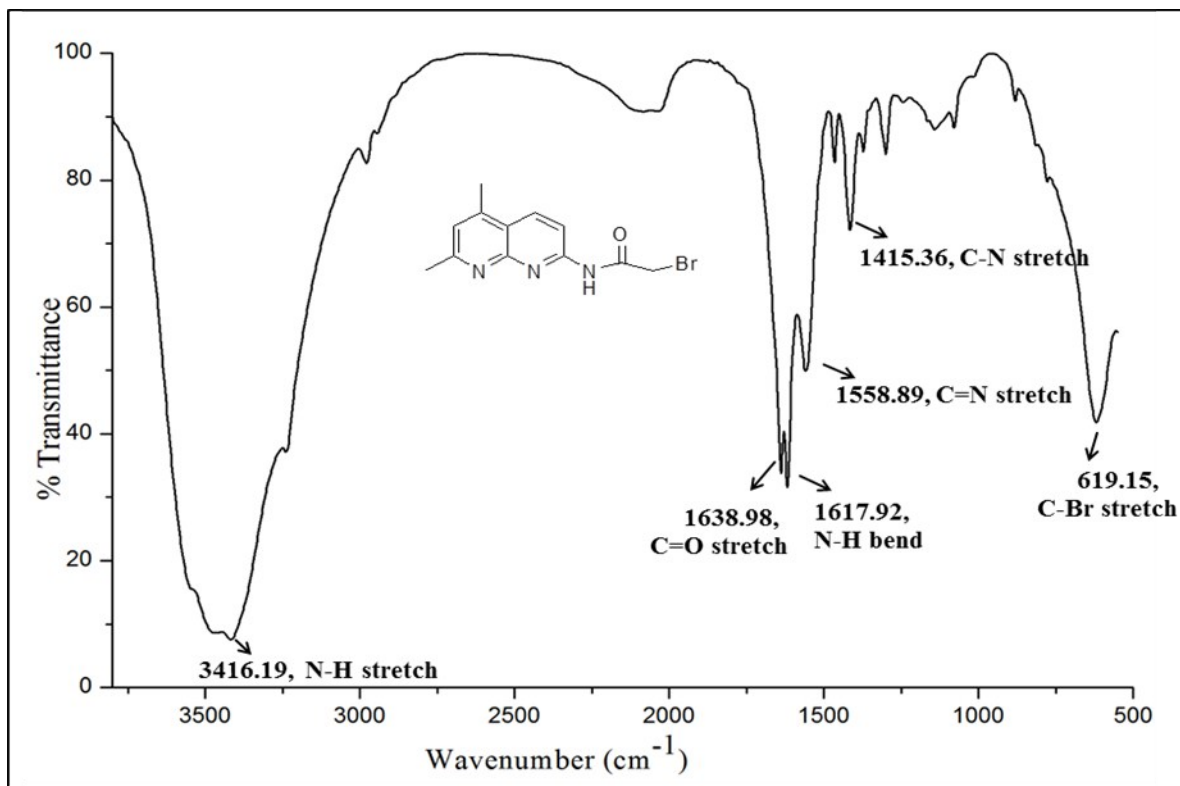


Figure S11. FT-IR spectrum of **nap-Br** in KBr pellet.

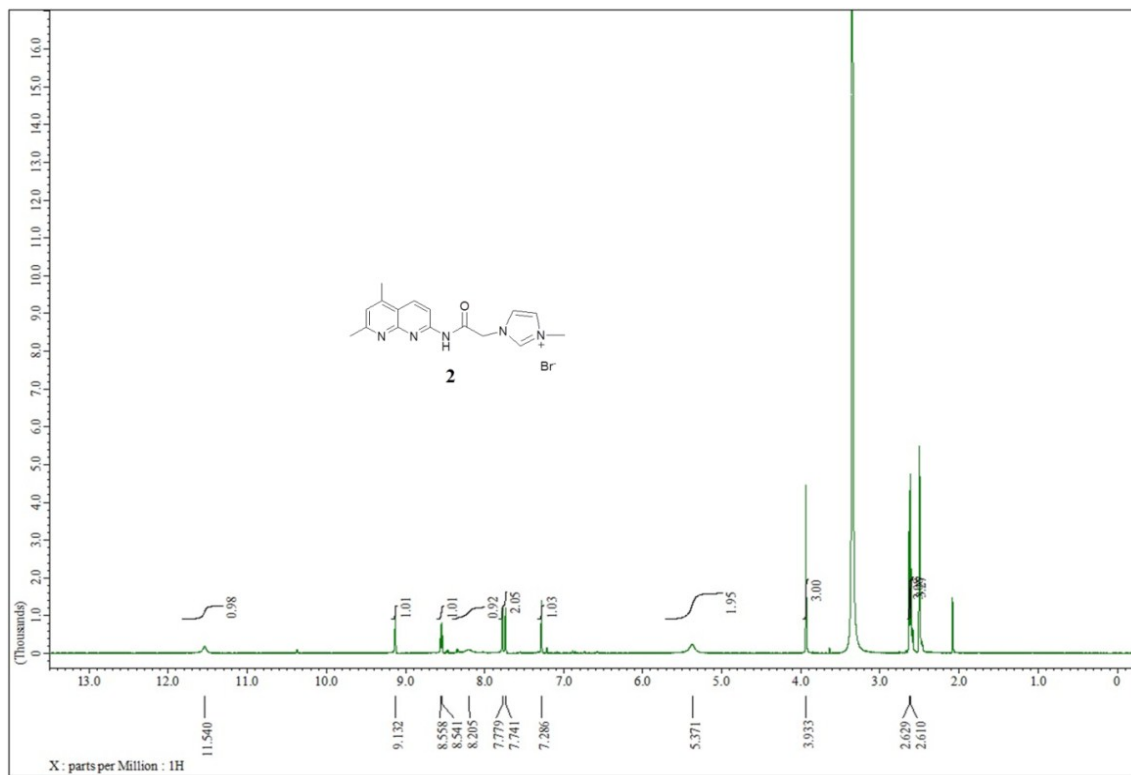


Figure S12. ^1H NMR spectrum of **2** in $\text{DMSO}-d_6$ at 298K.

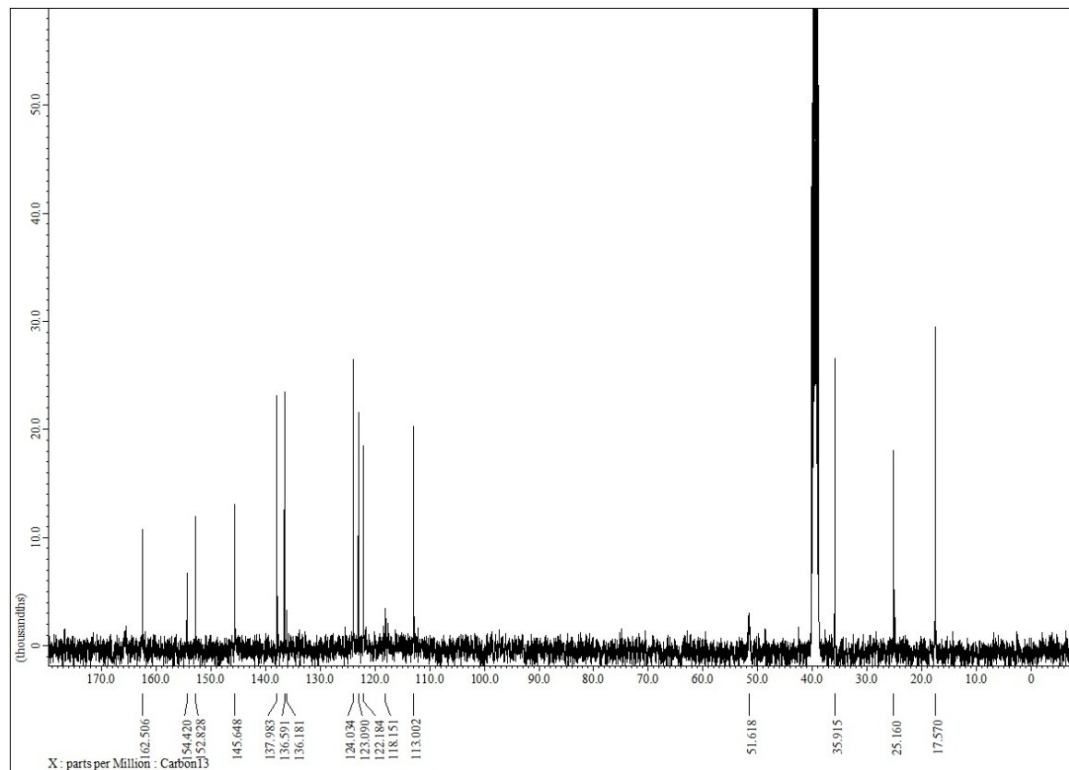


Figure S13. ^{13}C NMR spectrum of **2** in $\text{DMSO}-d_6$ at 298K.

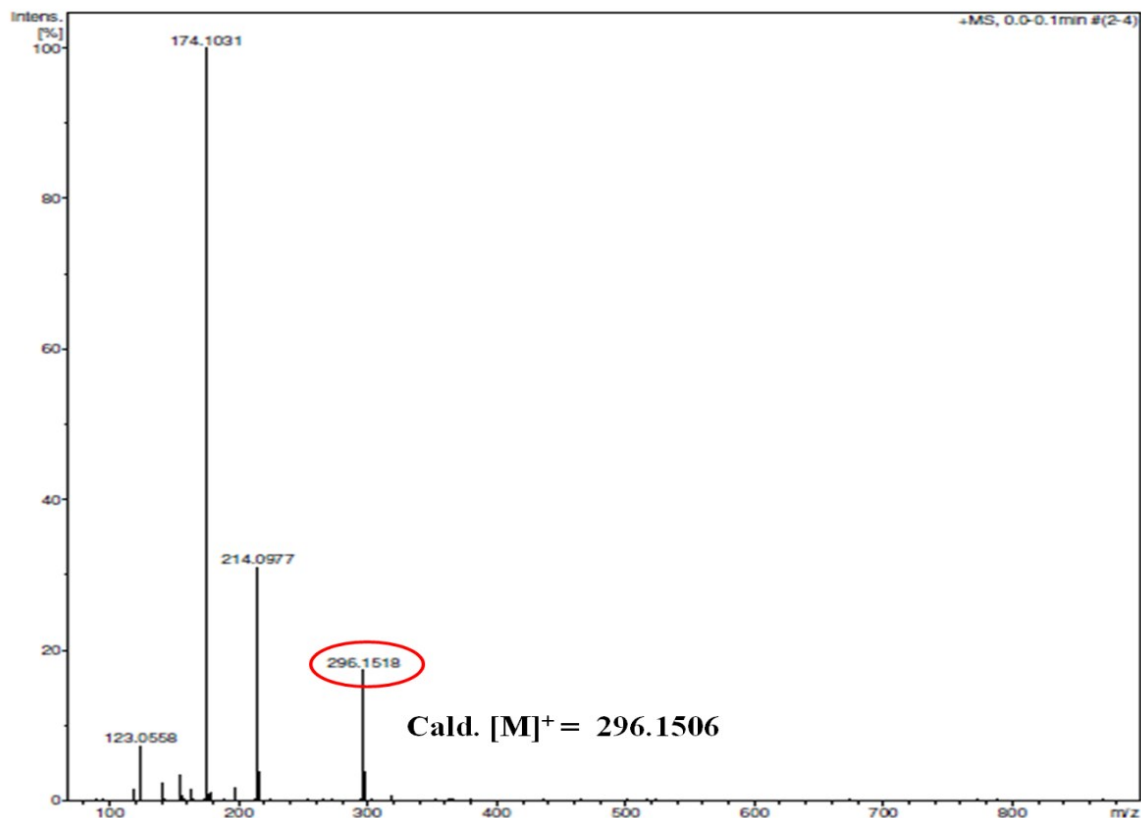


Figure S14. HRMS (ESI+) mass spectrum of **2** in CH_3CN .

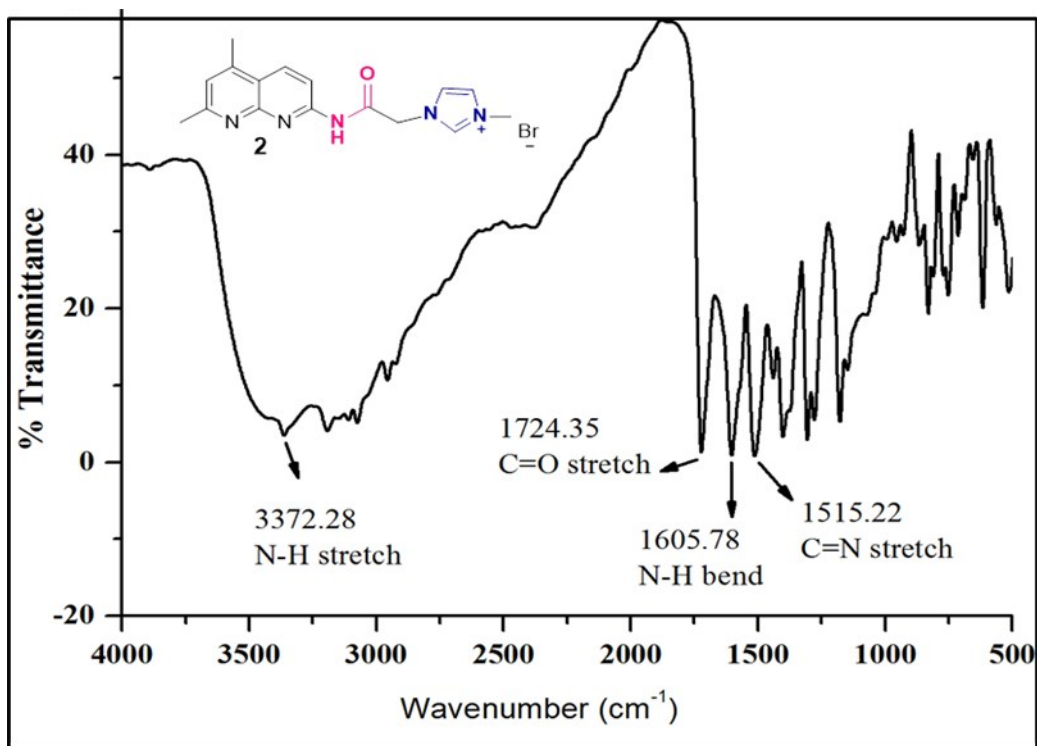


Figure S15. FT-IR spectrum of **2** in KBr pellet.

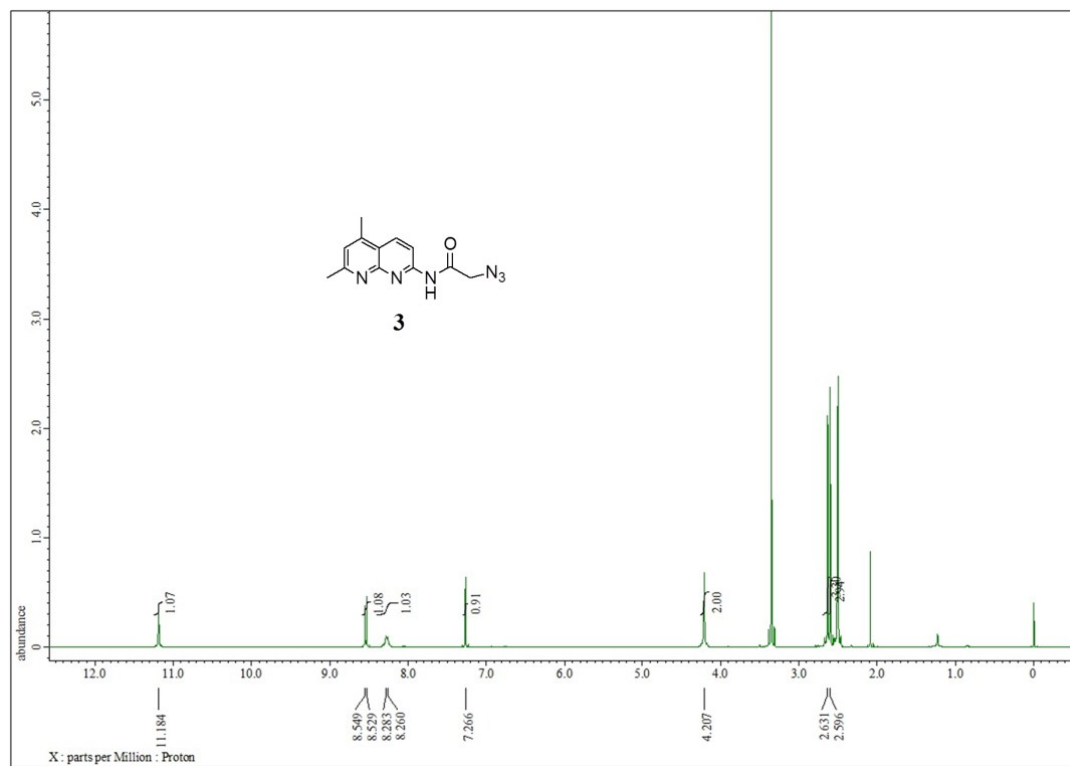


Figure S16. ^1H NMR spectrum of **3** in $\text{DMSO}-d_6$ at 298 K.

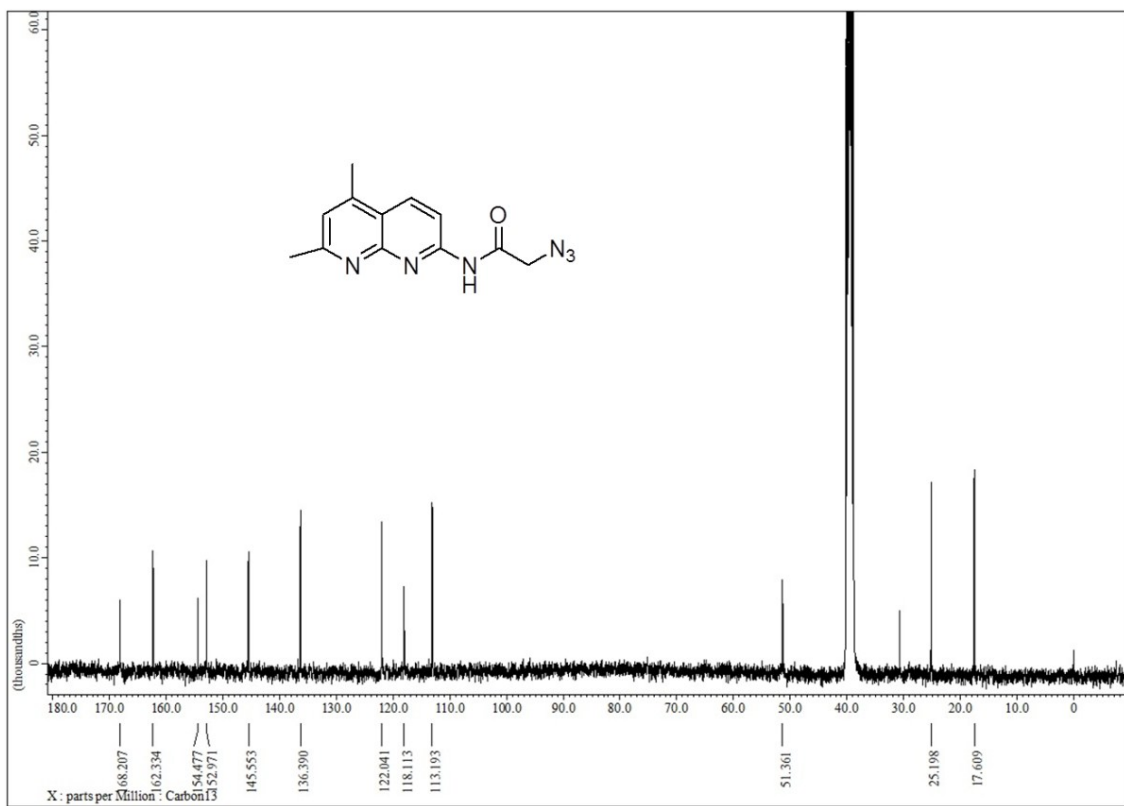


Figure S17. ^{13}C NMR spectrum of **3** in $\text{DMSO}-d_6$ at 298 K.

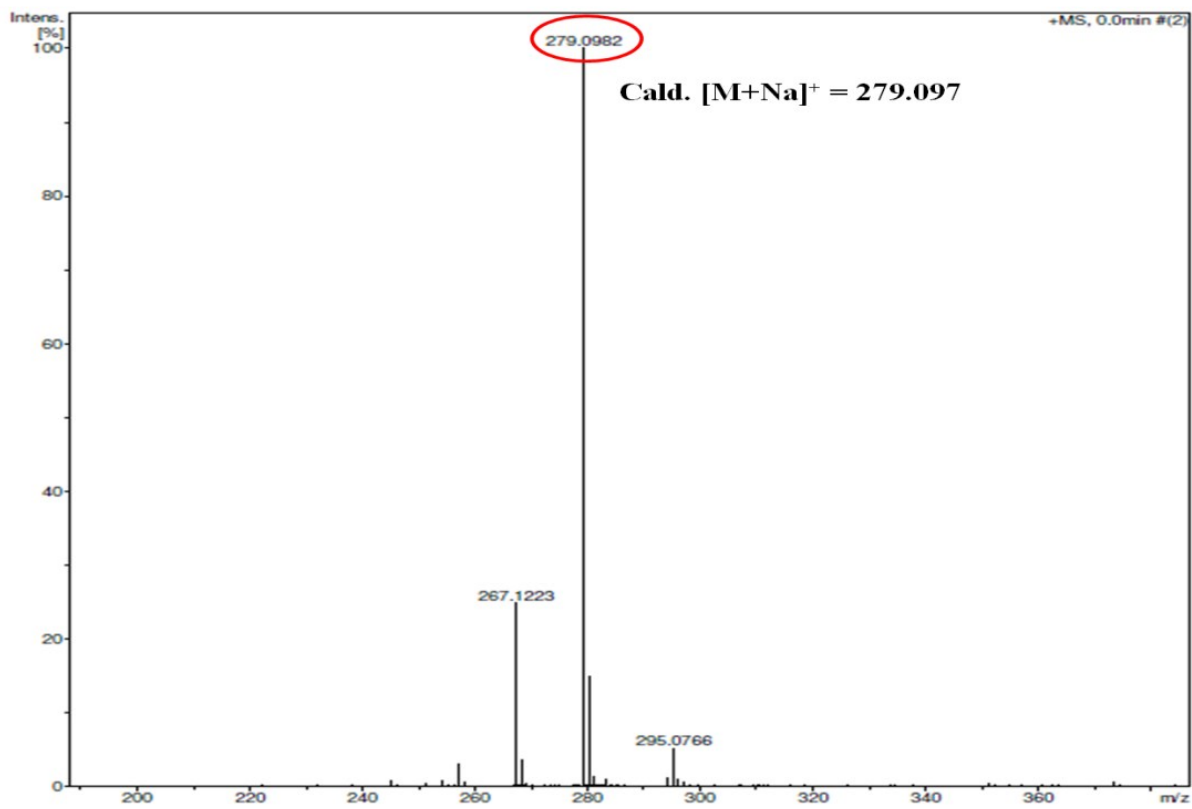


Figure S18. HRMS (ESI+) mass spectrum of **3** in CH_3CN .

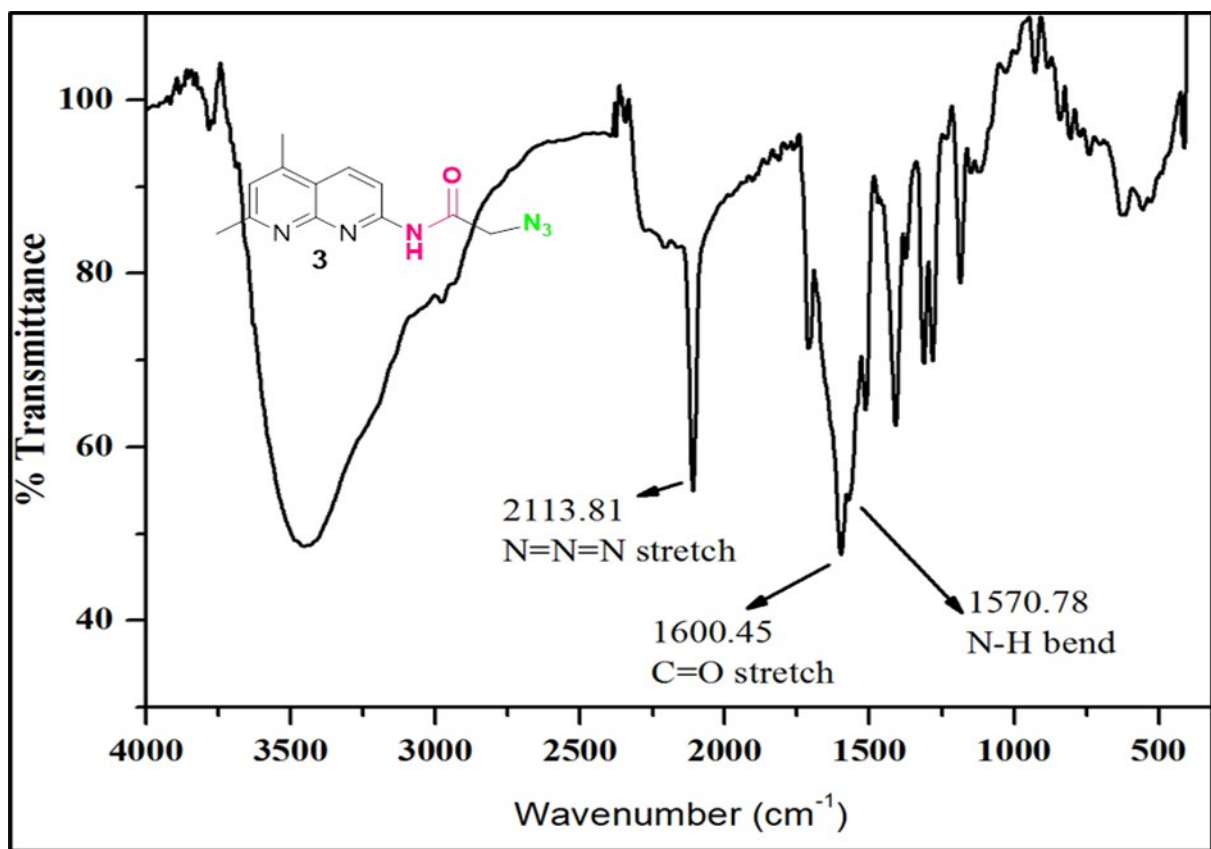


Figure S19. FT-IR spectrum of **3** in KBr pellet.

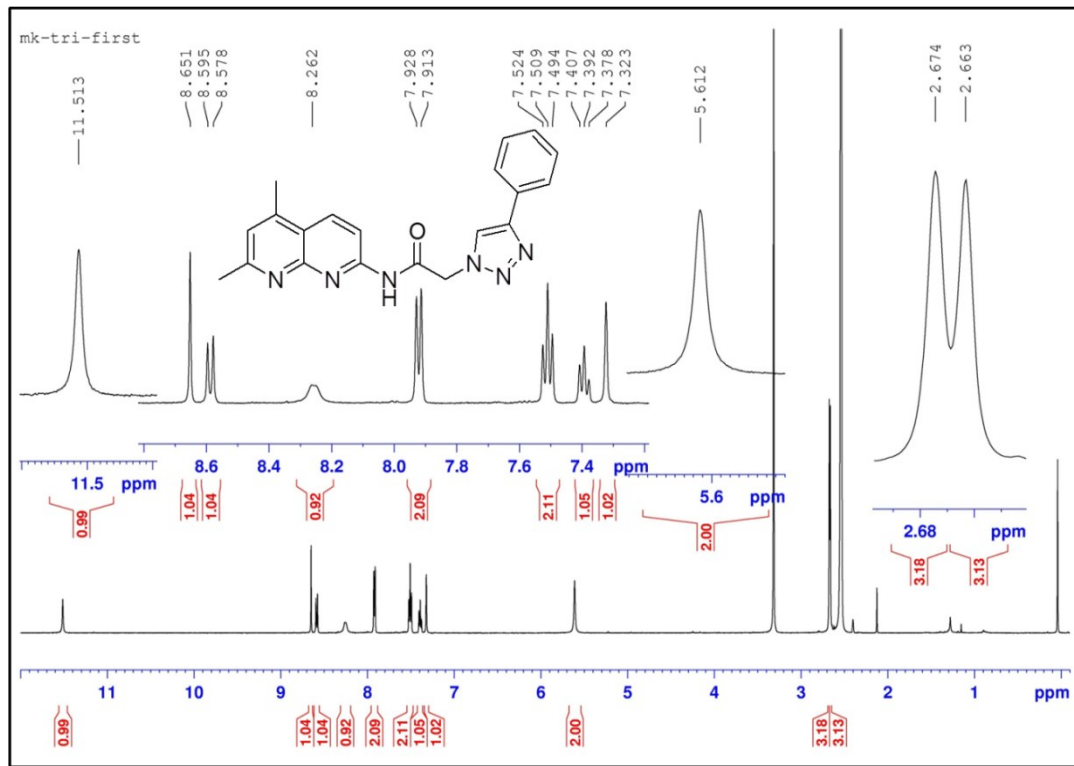


Figure S20. ¹H NMR spectrum of **4** in DMSO-*d*₆ at 298K.

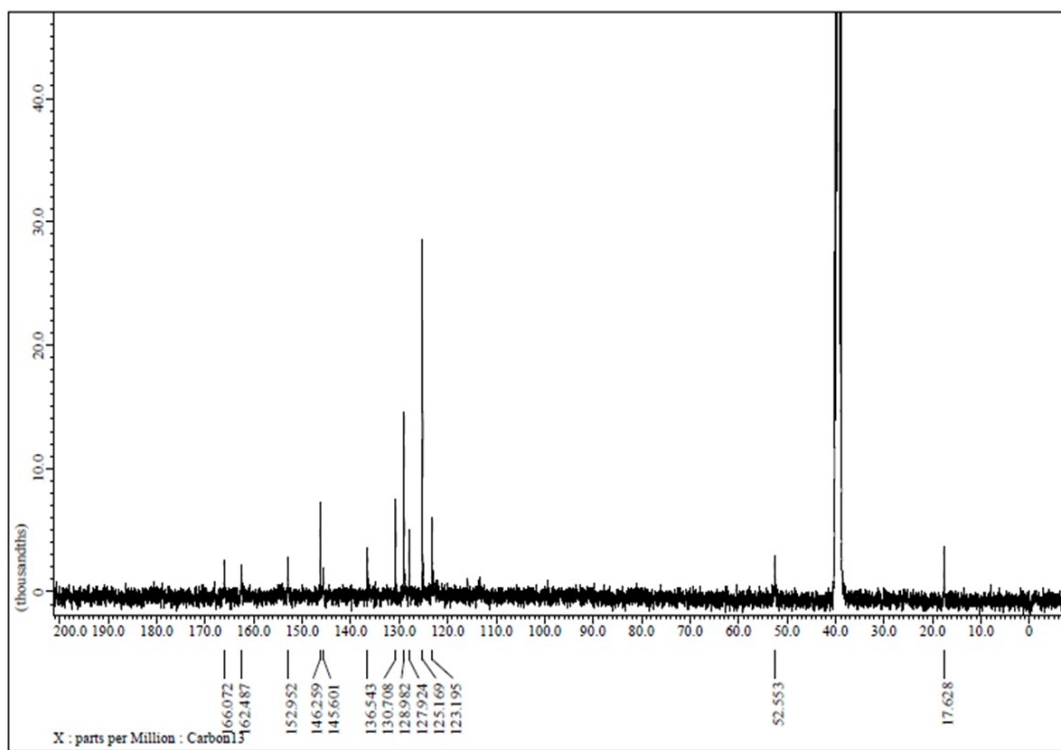


Figure S21. ^{13}C NMR spectrum of **4** in $\text{DMSO}-d_6$ at 298K.

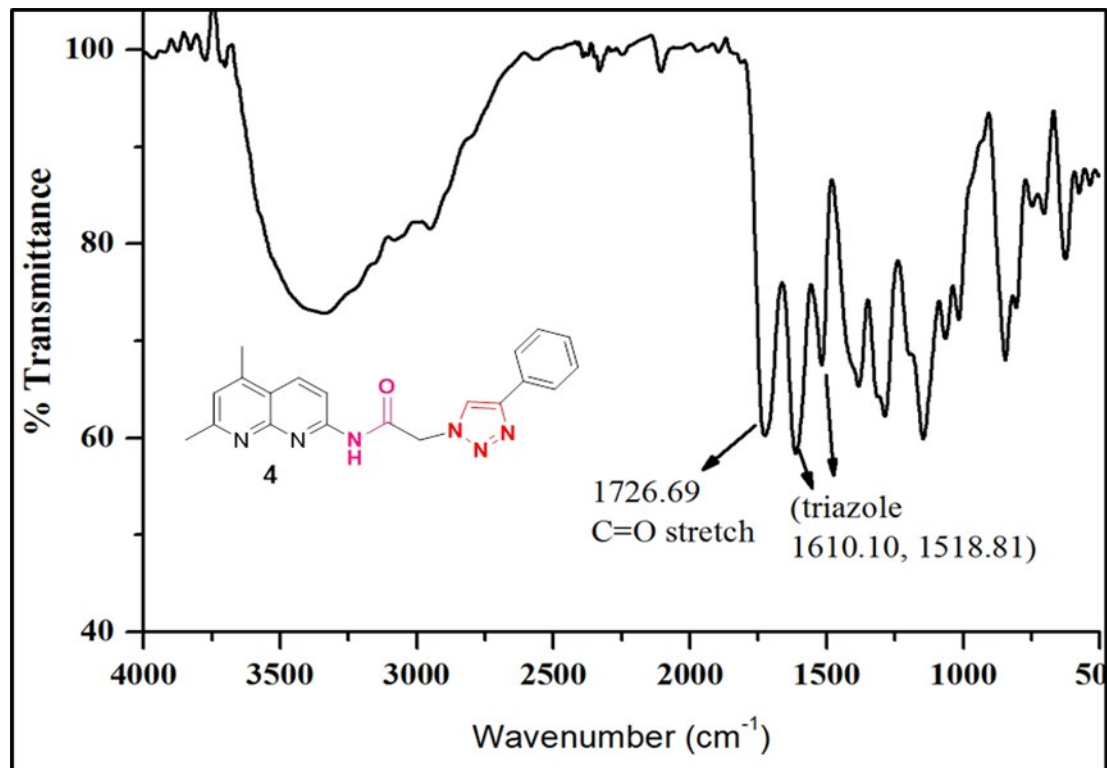


Figure S22. FT-IR spectrum of **4** in KBr pellet.

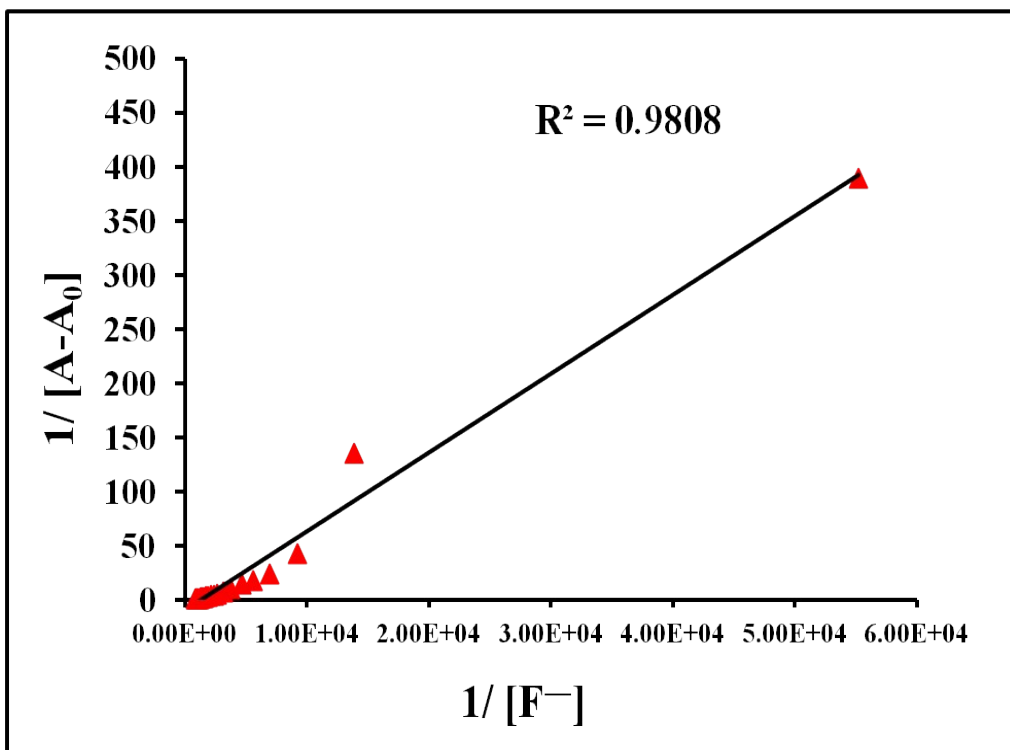


Figure S23. Benesi–Hildebrand plot for the titration of **1a** versus F^- ions showing a 1:1 binding stoichiometry.

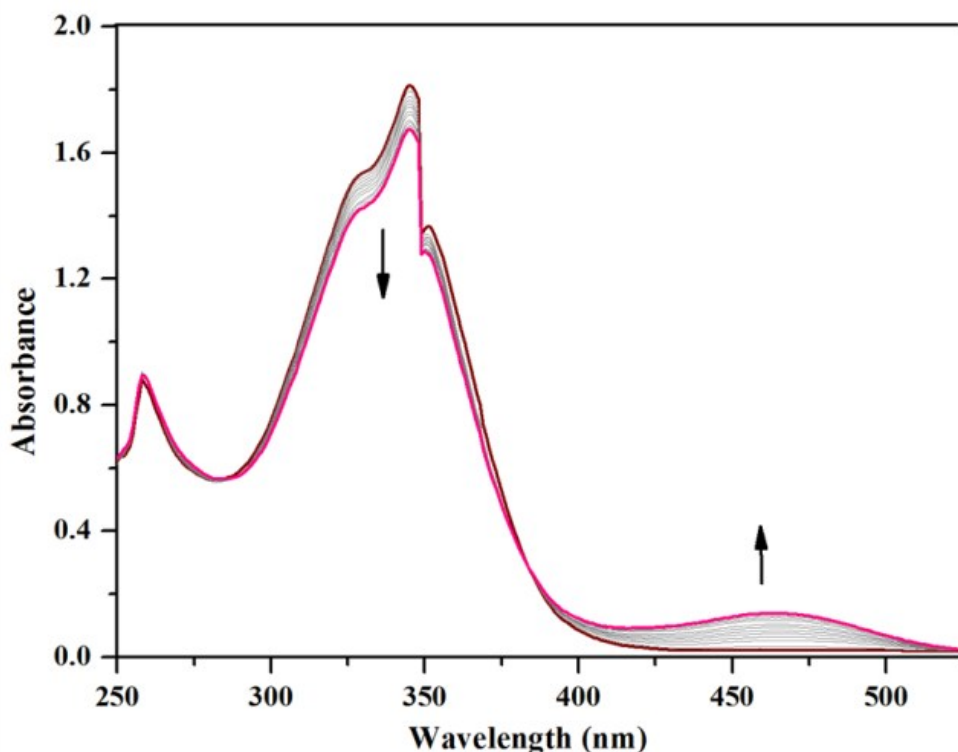


Figure S24. Change in UV-Vis spectrum for receptor **1a** at r. t. (4×10^{-5} M) in DMSO upon the addition of 0 to 4×10^{-3} M of cyanide ions.

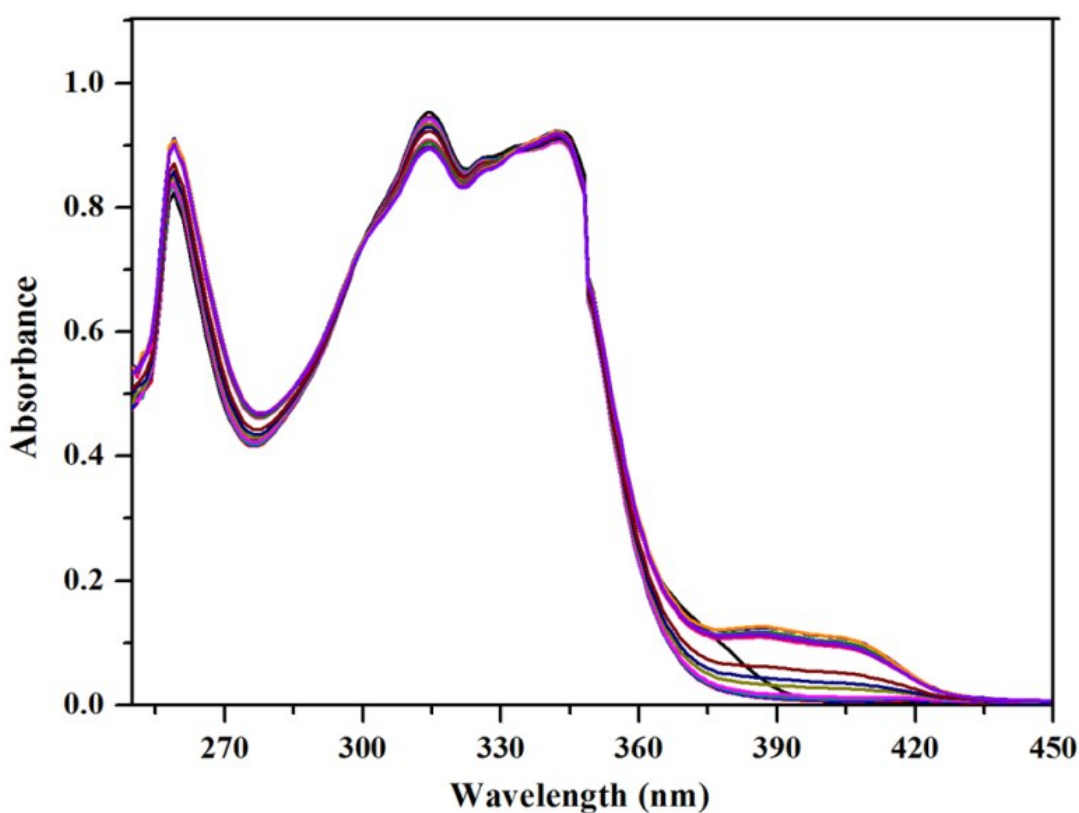


Figure S25. Change in UV-Vis spectrum for receptor **1b** at r. t. (4×10^{-5} M) in DMSO upon the addition of excess of fluoride ions.

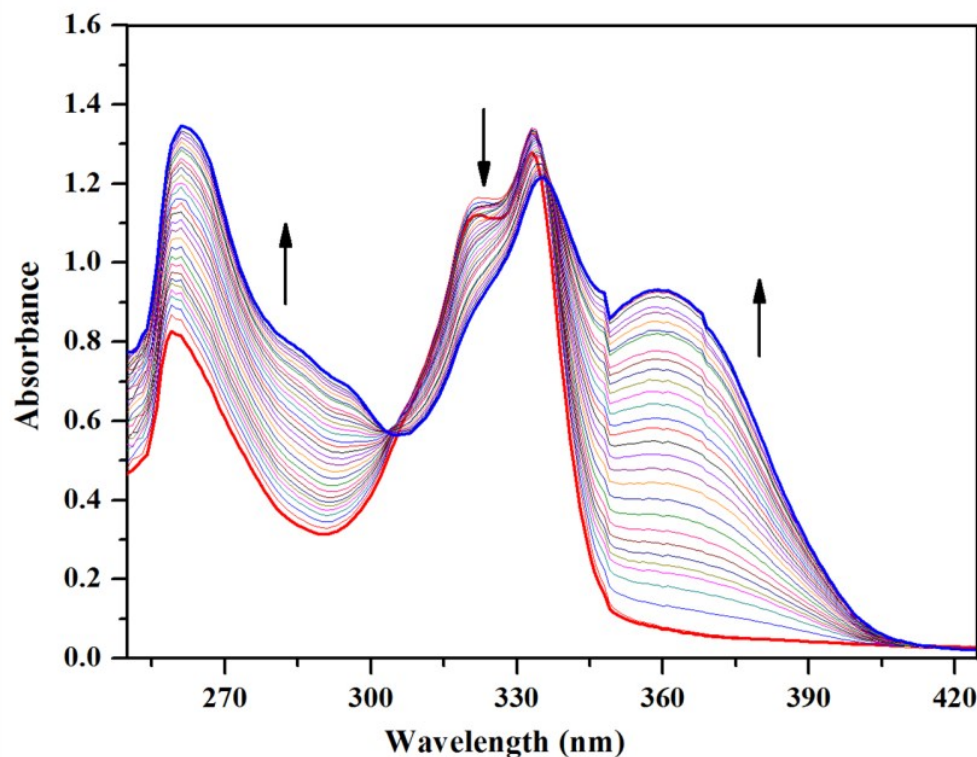


Figure S26. Change in UV-Vis spectrum for receptor **2** at r. t. (12×10^{-5} M) in DMSO upon the addition of 0 - 7.69×10^{-4} M (6.4 equiv.) of fluoride ions.

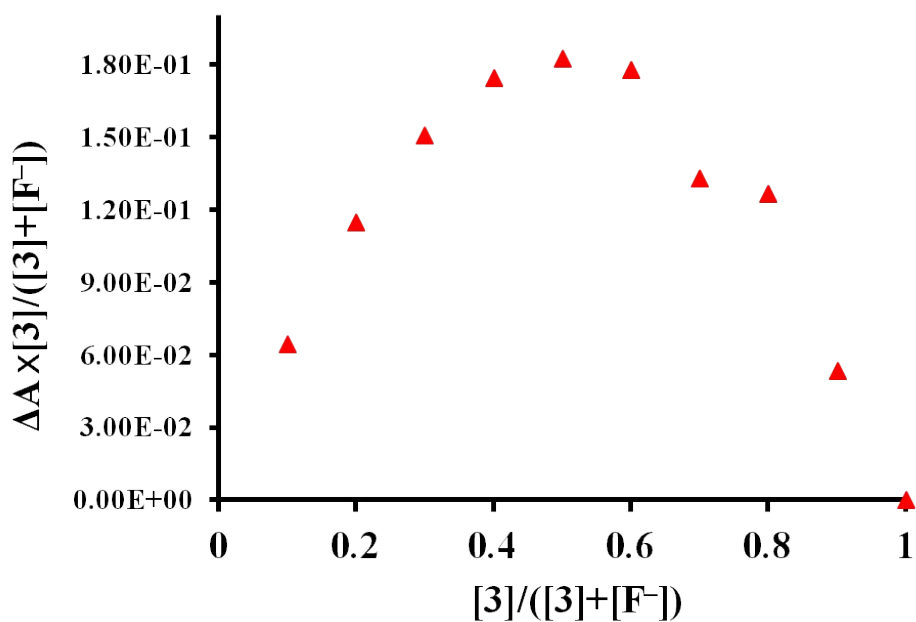


Figure S27. Job's plot for fluoride-2 interactions. The total ($[F^-] + [2]$) = 6.45×10^{-5} M.

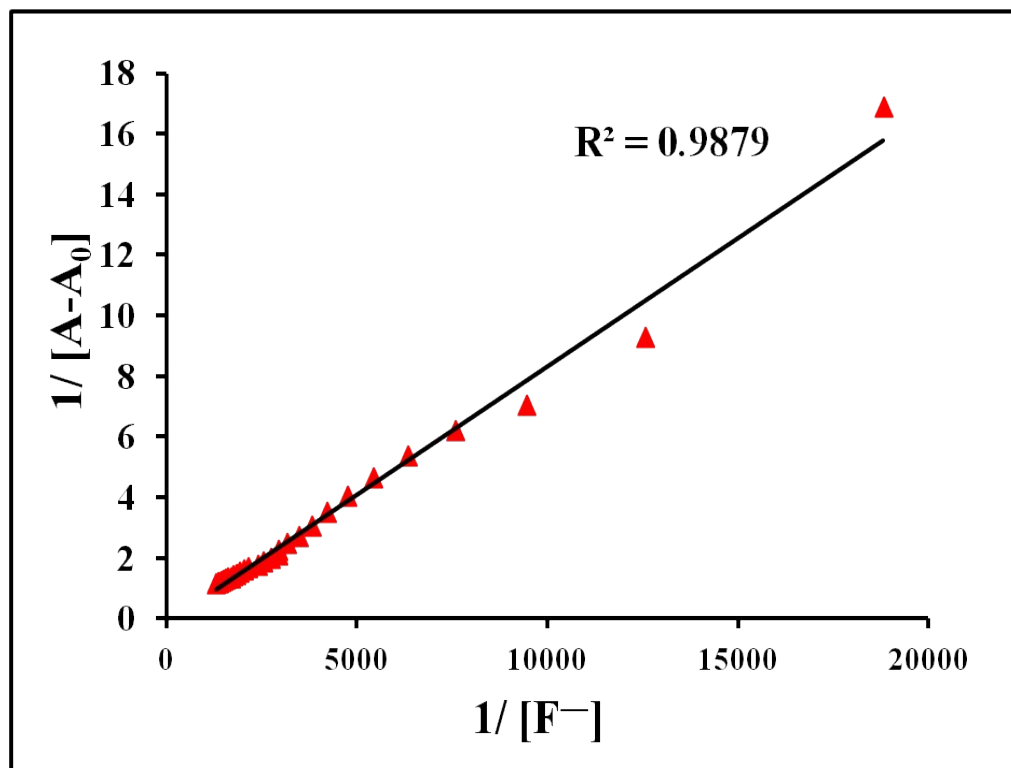


Figure S28. Benesi–Hildebrand plots for the titration of **2** versus F^- ions showing a 1:1 binding stoichiometry.

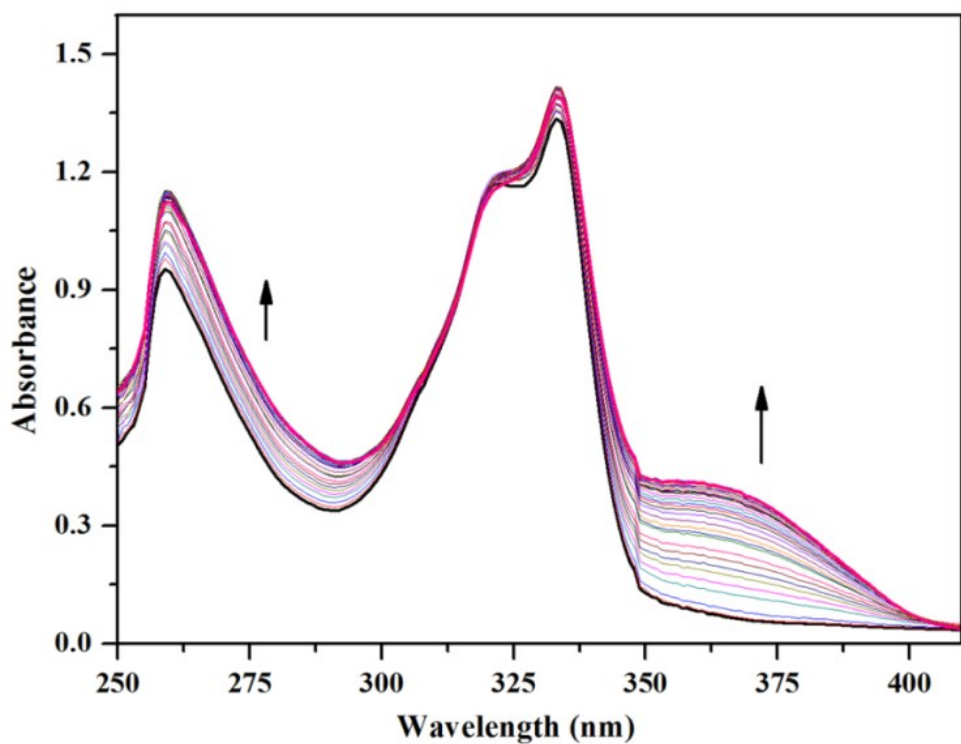


Figure S29. Change in UV-Vis spectrum for receptor **2** at r. t. (12×10^{-5} M) in DMSO upon the addition of 0 to 13.2×10^{-4} M (11 equiv.) of cyanide ions.

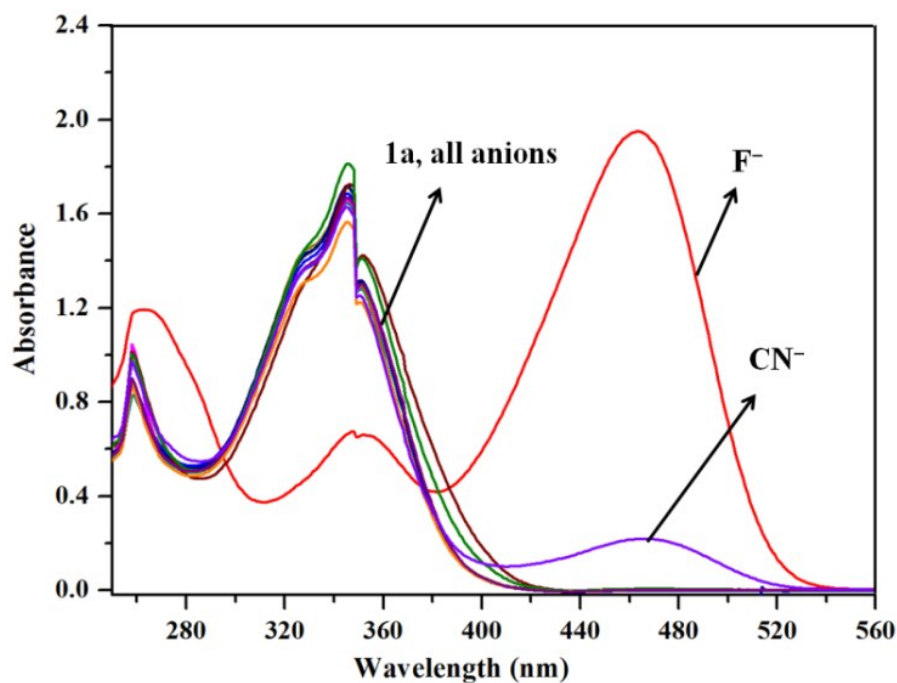


Figure S30. Absorption spectra of compound **1a** (4×10^{-5} M) upon addition of tetrabutylammonium F⁻, I⁻, Br⁻, OAc⁻, Cl⁻, H₂PO₄⁻, ClO₄⁻, HSO₄⁻, NO₃⁻, PF₆⁻ and CN⁻ (1.2×10^{-3} M) in DMSO.

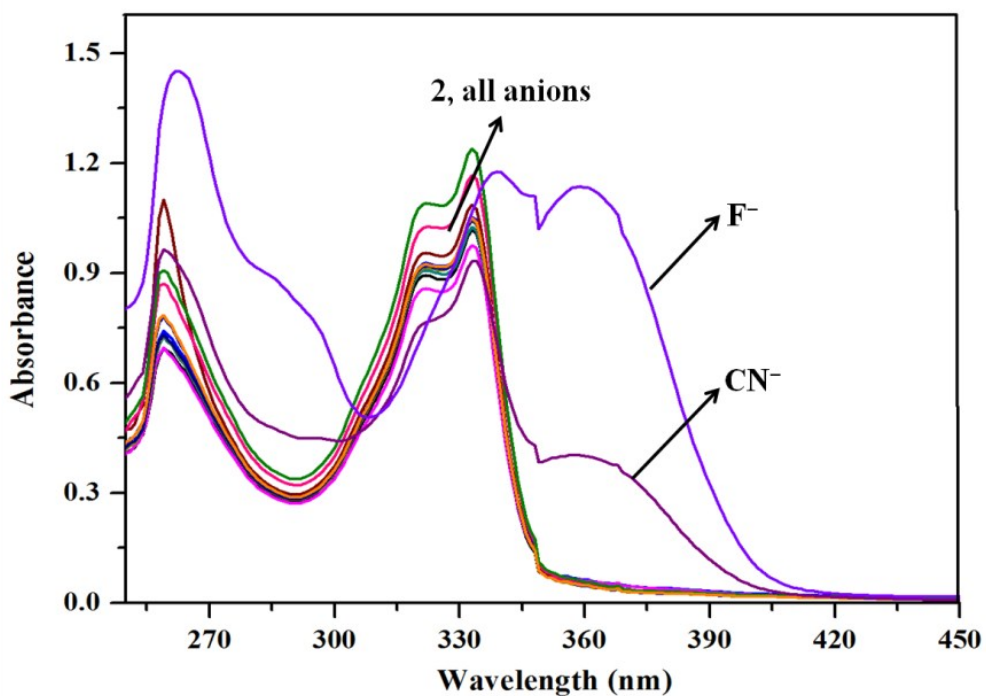


Figure S31. Absorption spectra of compound **2**(12 \times 10⁻⁵ M) upon addition of tetrabutylammonium F⁻, I⁻, Br⁻, OAc⁻, Cl⁻, H₂PO₄⁻, ClO₄⁻, HSO₄⁻, NO₃⁻, PF₆⁻ and CN⁻ (8 equiv.) in DMSO.

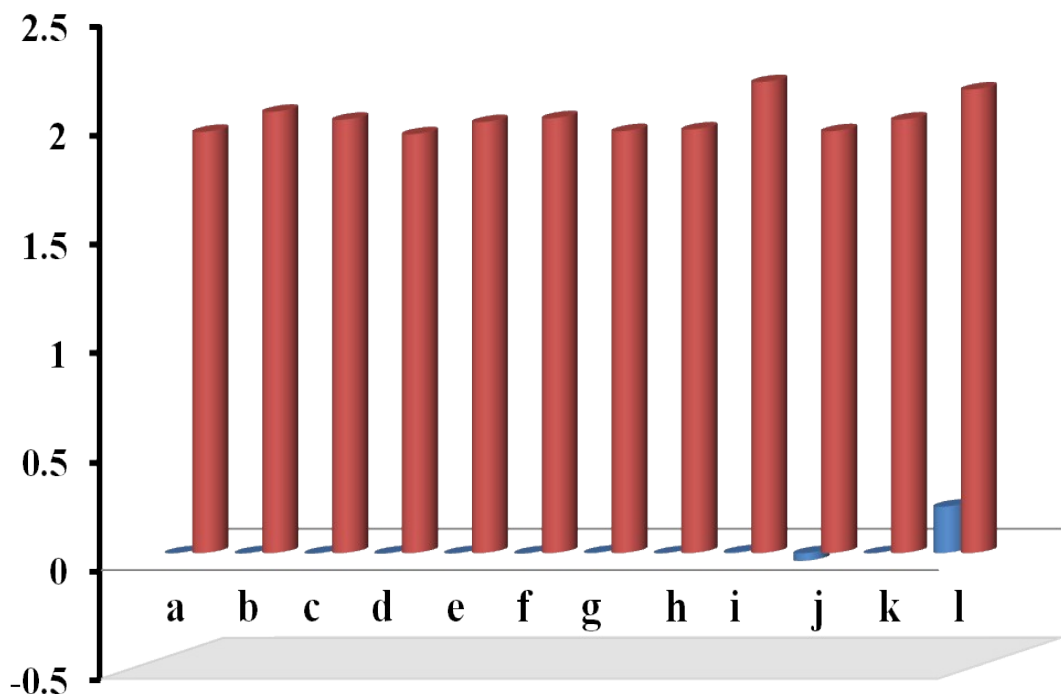


Figure S32. Selectivity of anions at wavelength 462 nm in a solution having **1a** + anions (blue bar) and **1a** + anions + F⁻ (red bar) observed using UV-Vis spectral studies. (a) all X⁻ (b) Br⁻ (c) HSO₄⁻ (d) I⁻ (e) BH₄⁻ (f) ClO₄⁻ (g) CH₃COO⁻ (h) PF₆⁻ (i) H₂PO₄⁻ (j) NO₃⁻ (k) Cl⁻ (l) CN⁻.

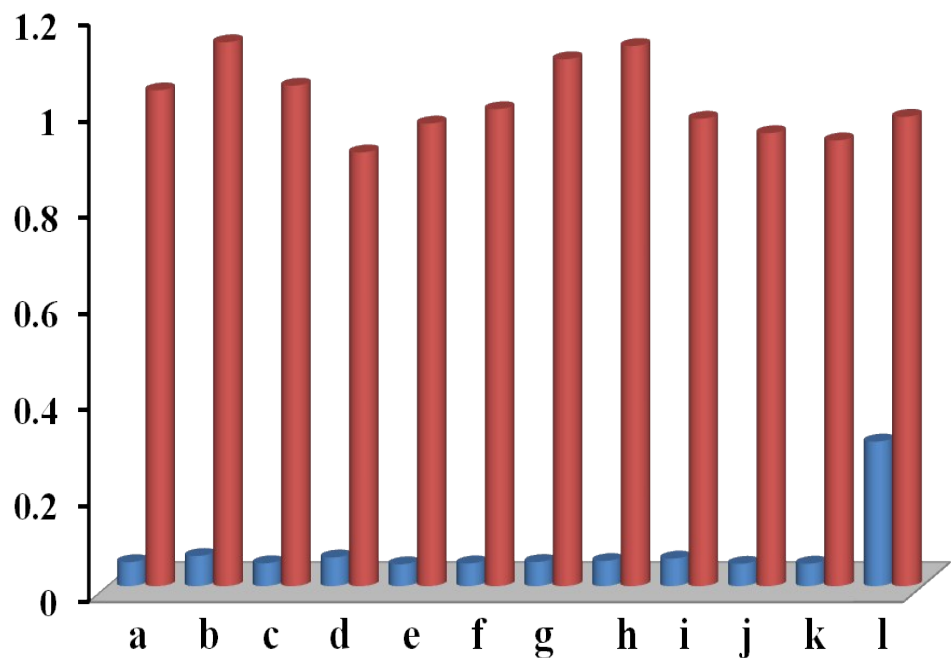


Figure S33. Selectivity of anions at wavelength 360 nm in a solution having **2** + anions (blue bar) and **2** + anions + F^- (red bar) observed using UV-Vis spectral studies. (a) all X^- (b) Br^- (c) HSO_4^- (d) I^- (e) BH_4^- (f) ClO_4^- (g) CH_3COO^- (h) PF_6^- (i) H_2PO_4^- (j) NO_3^- (k) Cl^- (l) CN^- .

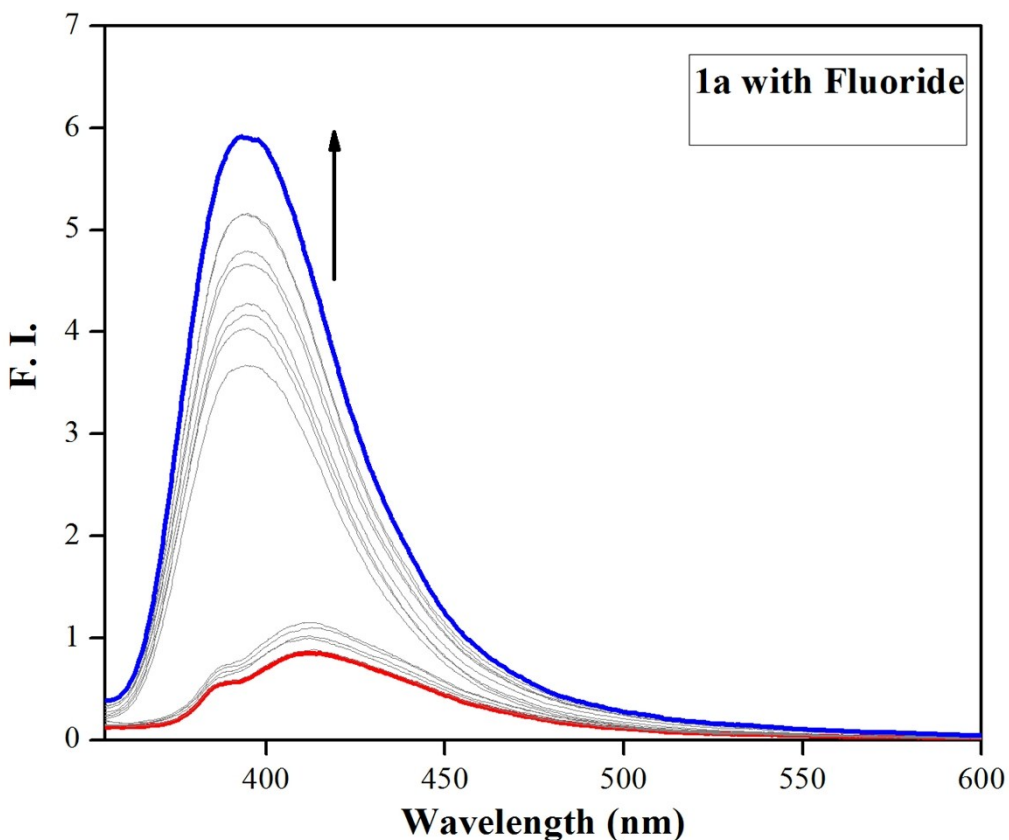


Figure S34. Fluorescence changes of **1a** (1×10^{-5} M) upon the addition of tetrabutylammonium fluoride (0- 3×10^{-4} M, 30 equiv.) in DMSO.

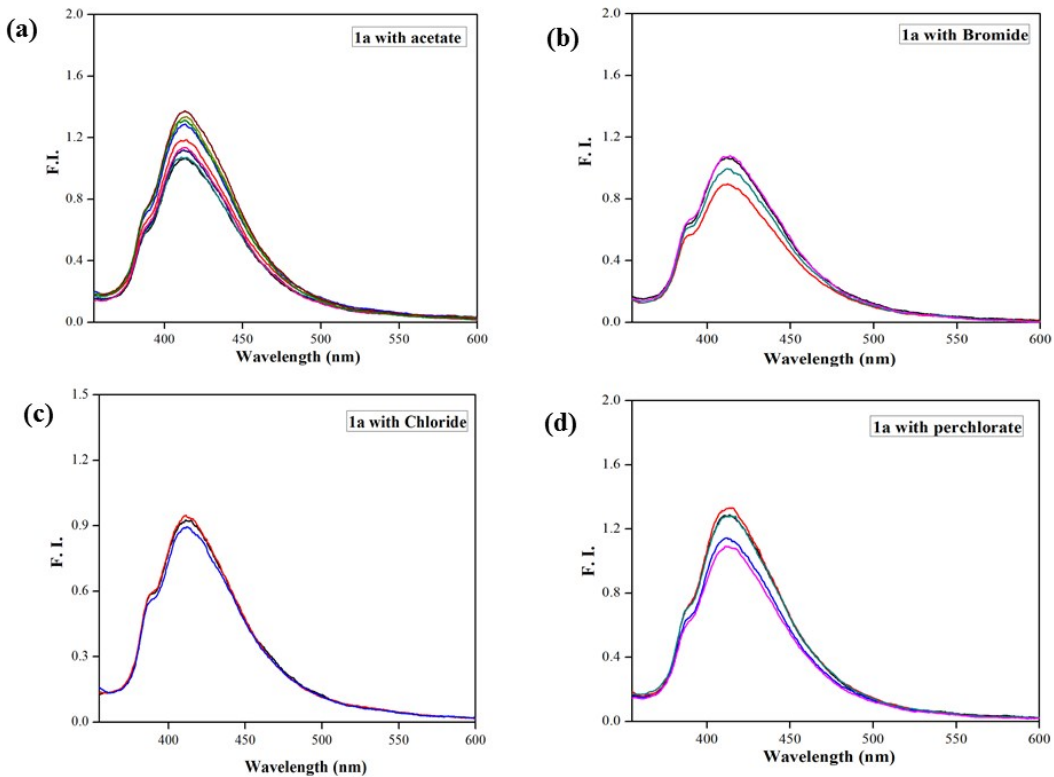


Figure S35. Fluorescence changes of **1a** (1×10^{-5} M) upon the addition of different anions (a) CH_3COO^- (b) Br^- (c) Cl^- and (d) ClO_4^- from 0 - 60 equiv. in DMSO at 298 K.

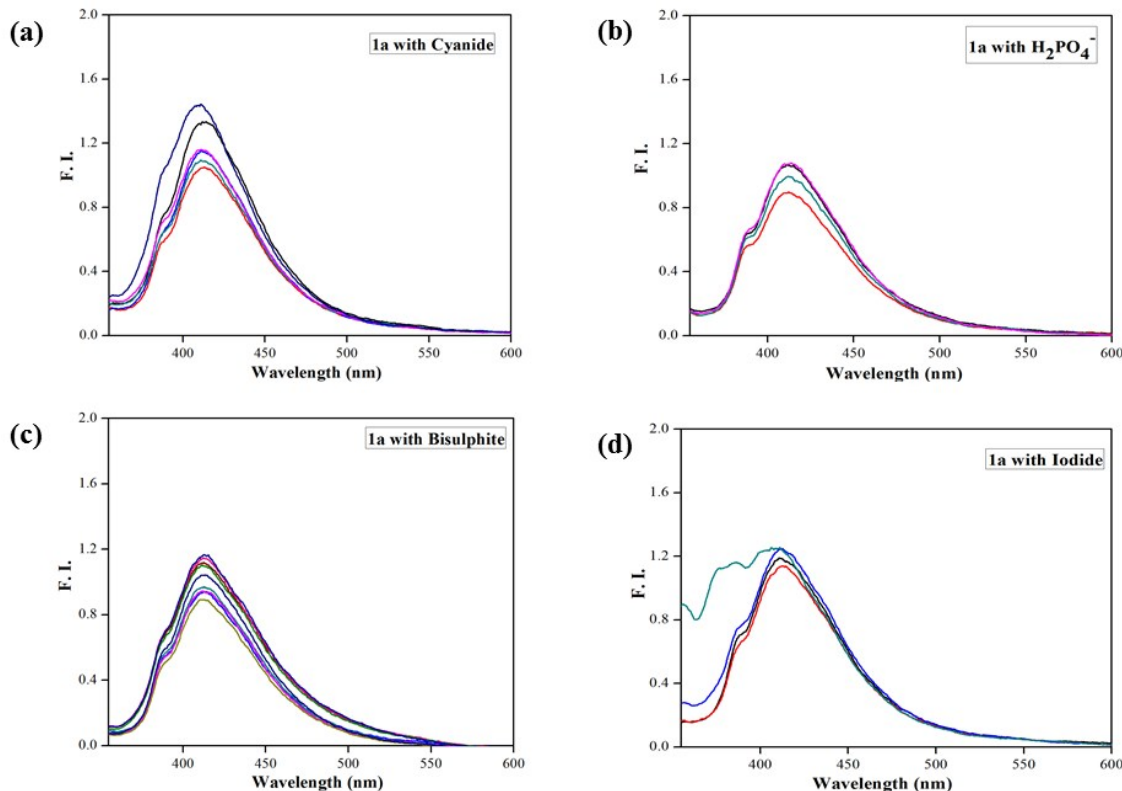


Figure S36. Fluorescence changes of **1a** (1×10^{-5} M) upon the addition of different anions (a) CN^- (b) H_2PO_4^- (c) HSO_4^- and (d) I^- from 0 - 60 equiv. in DMSO at 298 K.

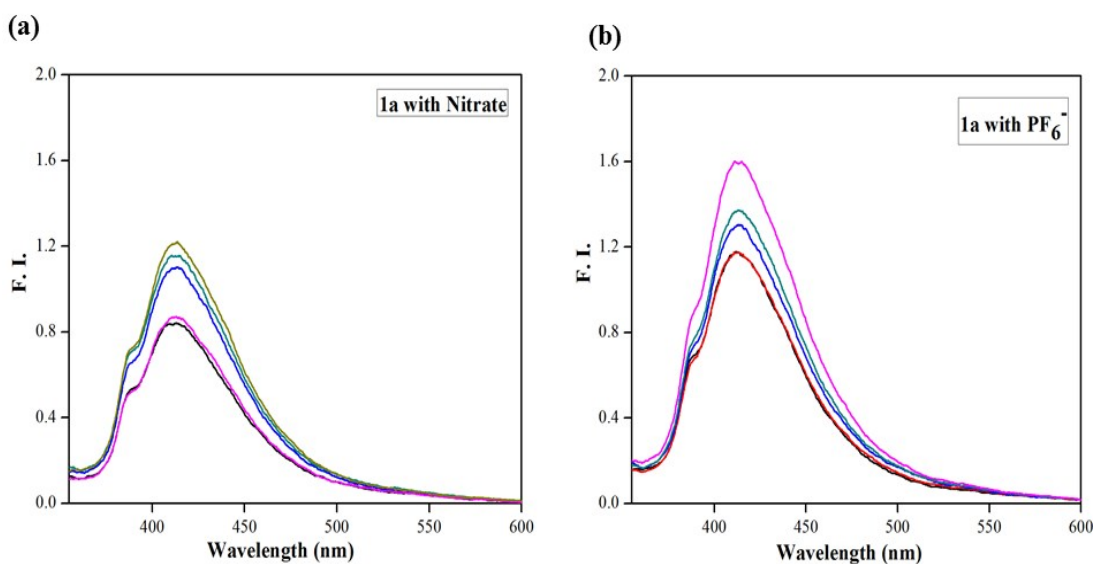


Figure S37. Fluorescence changes of **1a** (1×10^{-5} M) upon the addition of different anions (a) NO_3^- and (b) PF₆⁻ from 0 - 60 equiv. in DMSO at 298 K.

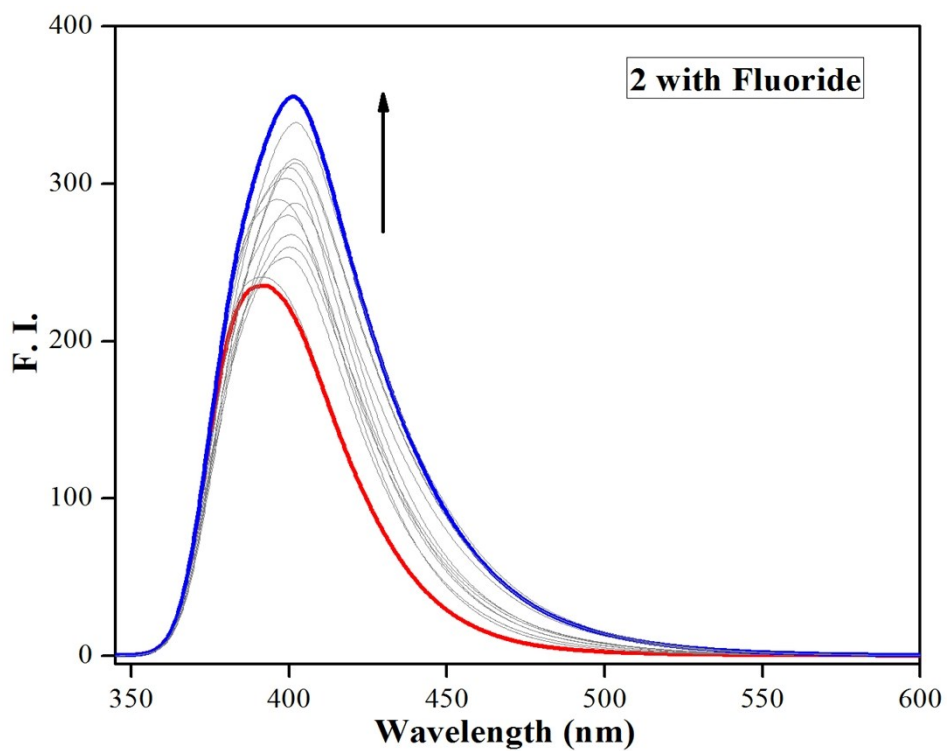


Figure S38. Fluorescence changes for receptor **2** at r. t. (1×10^{-5} M) in DMSO upon the addition of 0 – 6.4×10^{-5} M (6.4 equiv.) of fluoride ions.

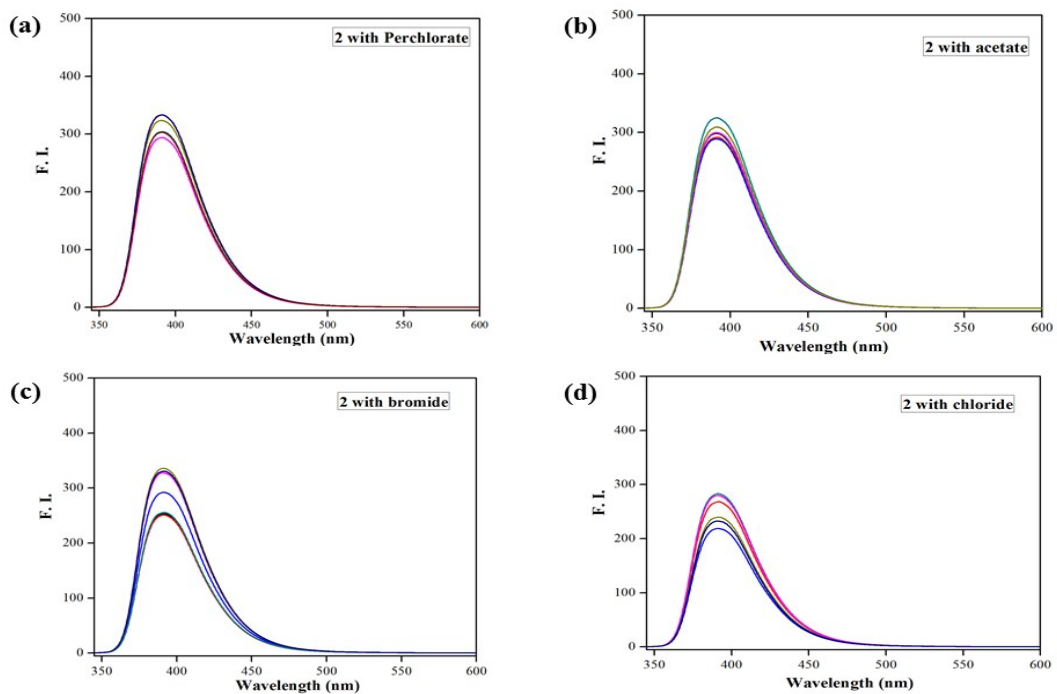


Figure S39. Fluorescence changes of **2** (1×10^{-5} M) upon the addition of different anions (a) ClO_4^- (b) CH_3COO^- (c) Br^- and (d) Cl^- from 0 - 20 equiv. in DMSO at 298 K.

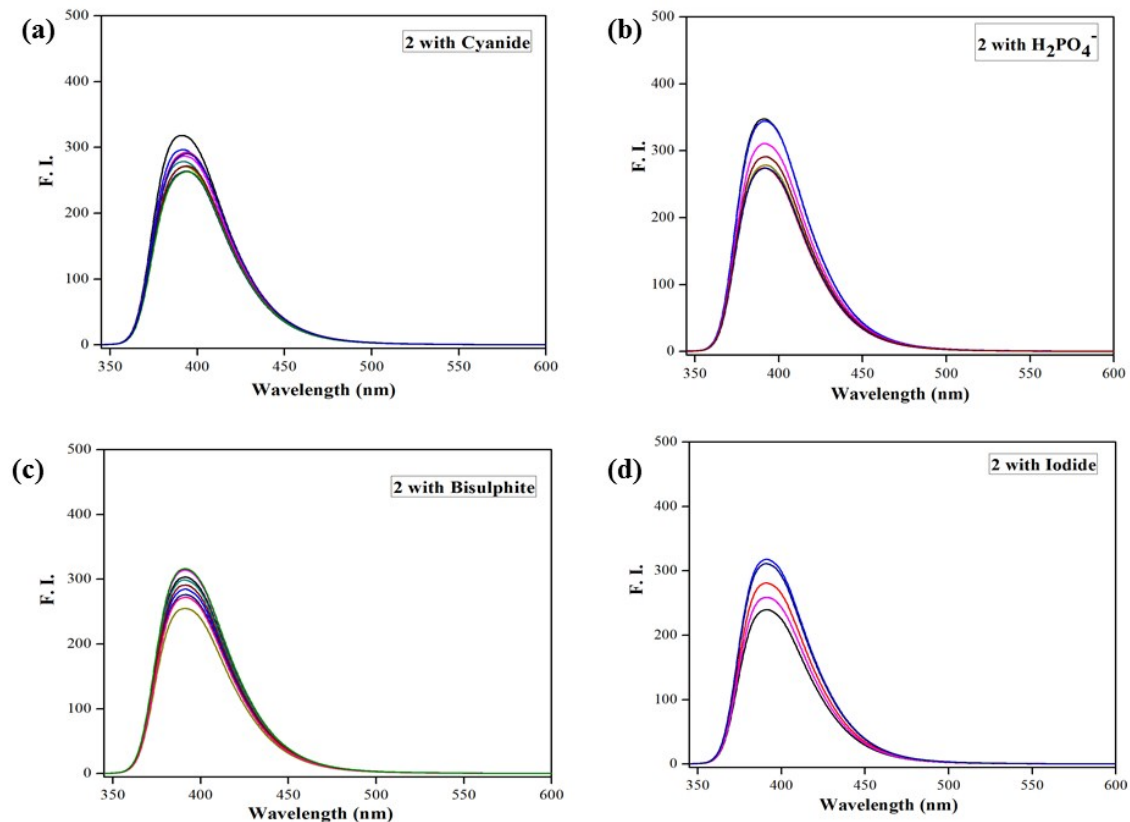


Figure S40. Fluorescence changes of **2** (1×10^{-5} M) upon the addition of different anions (a) CN^- (b) H_2PO_4^- (c) HSO_4^- and (d) I^- from 0 - 20 equiv. in DMSO at 298 K.

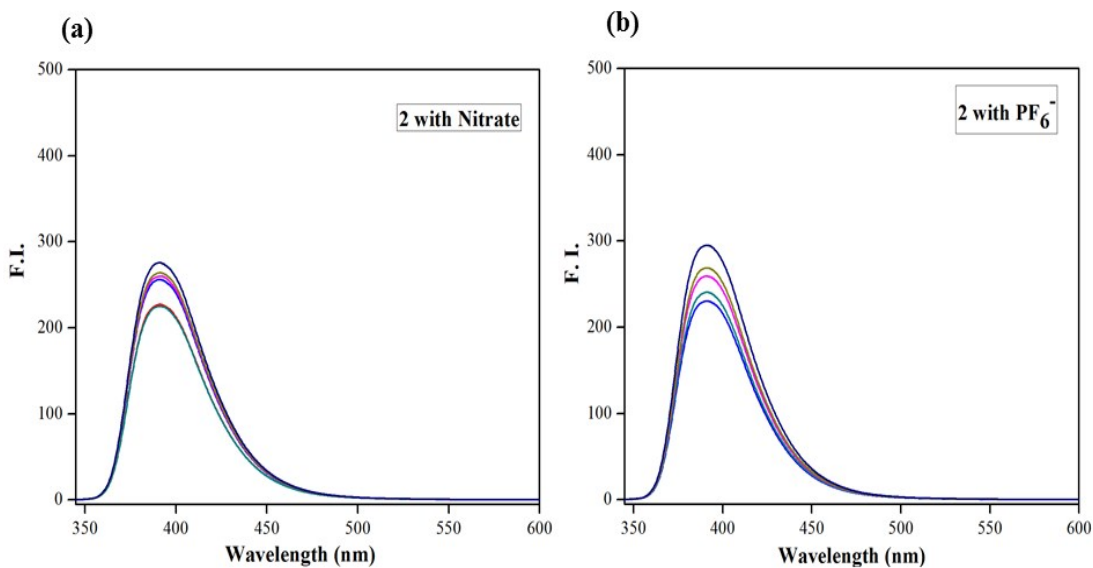


Figure S41. Fluorescence changes of **2** (1×10^{-5} M) upon the addition of different anions (a) NO_3^- and (b) PF_6^- from 0 - 20 equiv. in DMSO at 298 K.

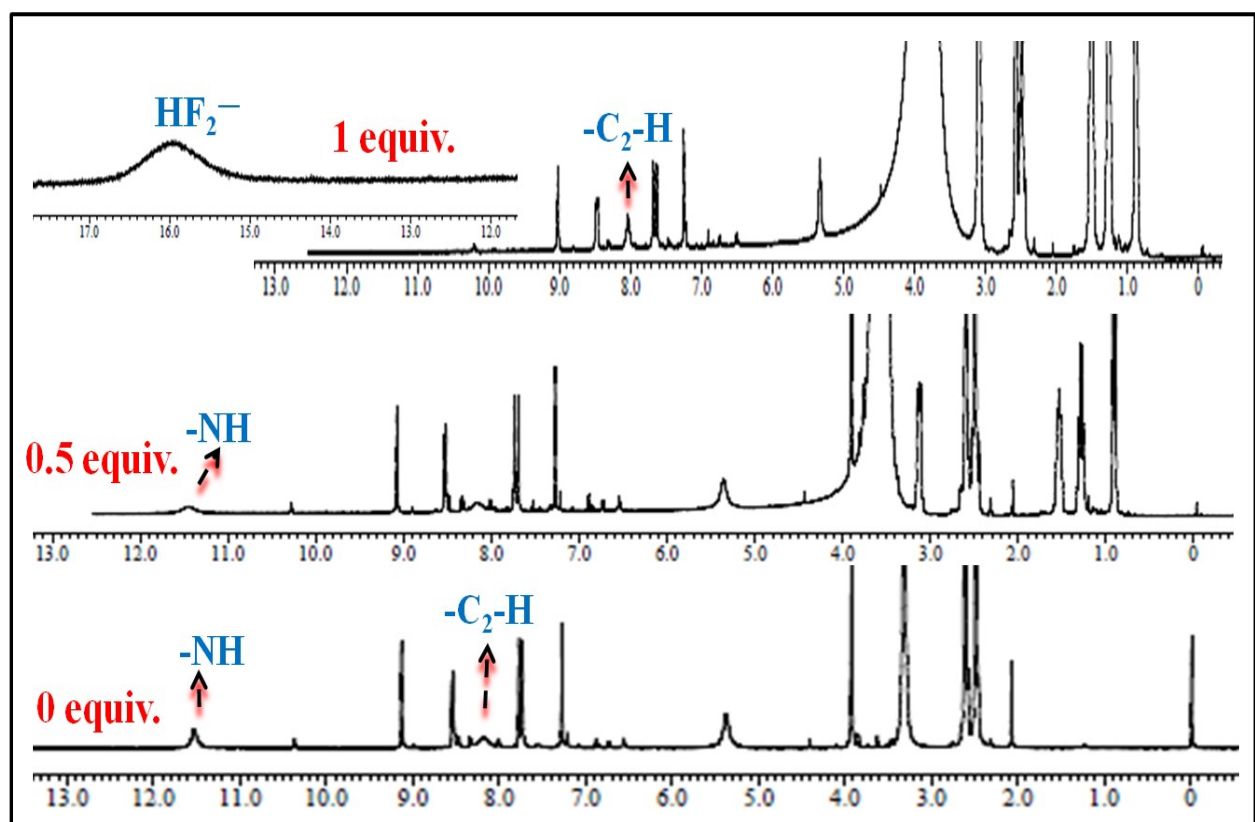


Figure S42. ¹H-NMR Titration of a 5×10^{-3} M solution of **2** in DMSO-*d*₆ with increasing concentration of F⁻ ions.

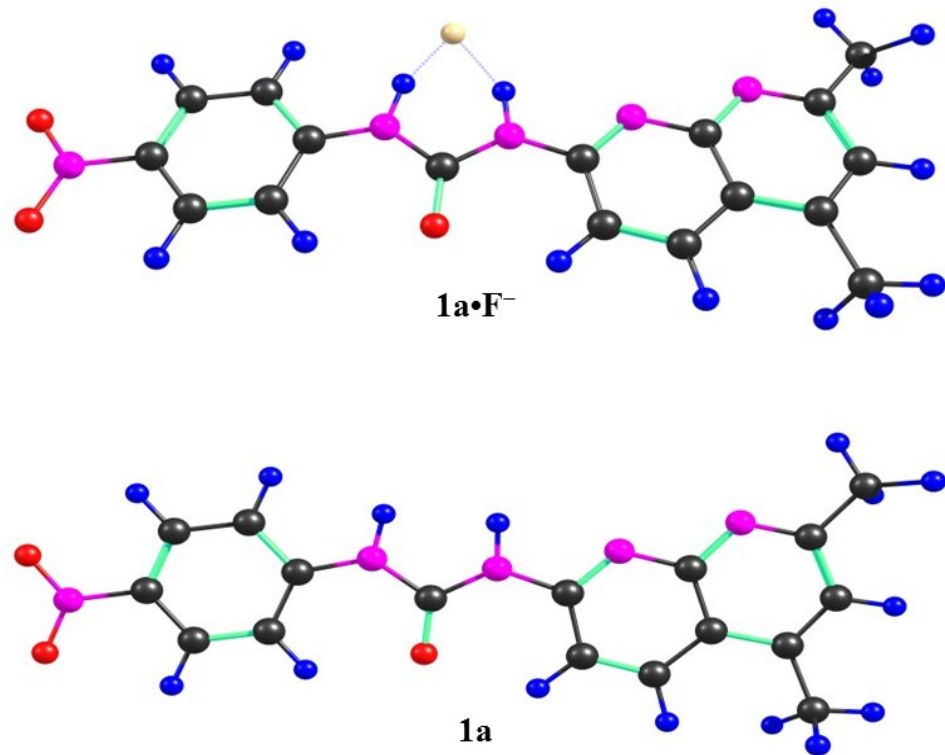


Figure S43. DFT optimized structures of $1\mathbf{a}$ and $1\mathbf{a}\cdot\mathbf{F}^-$ in DMSO.

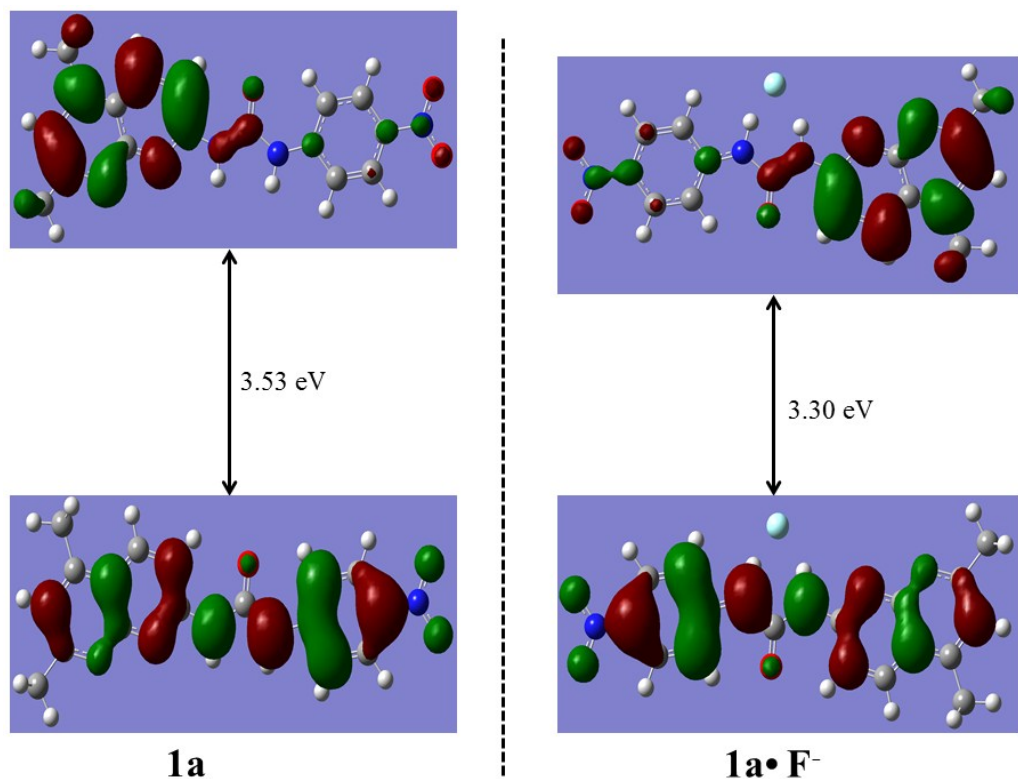


Figure S44. HOMO-LUMO energy gaps for $1\mathbf{a}$ and $1\mathbf{a}\cdot\mathbf{F}^-$ complex in DMSO.

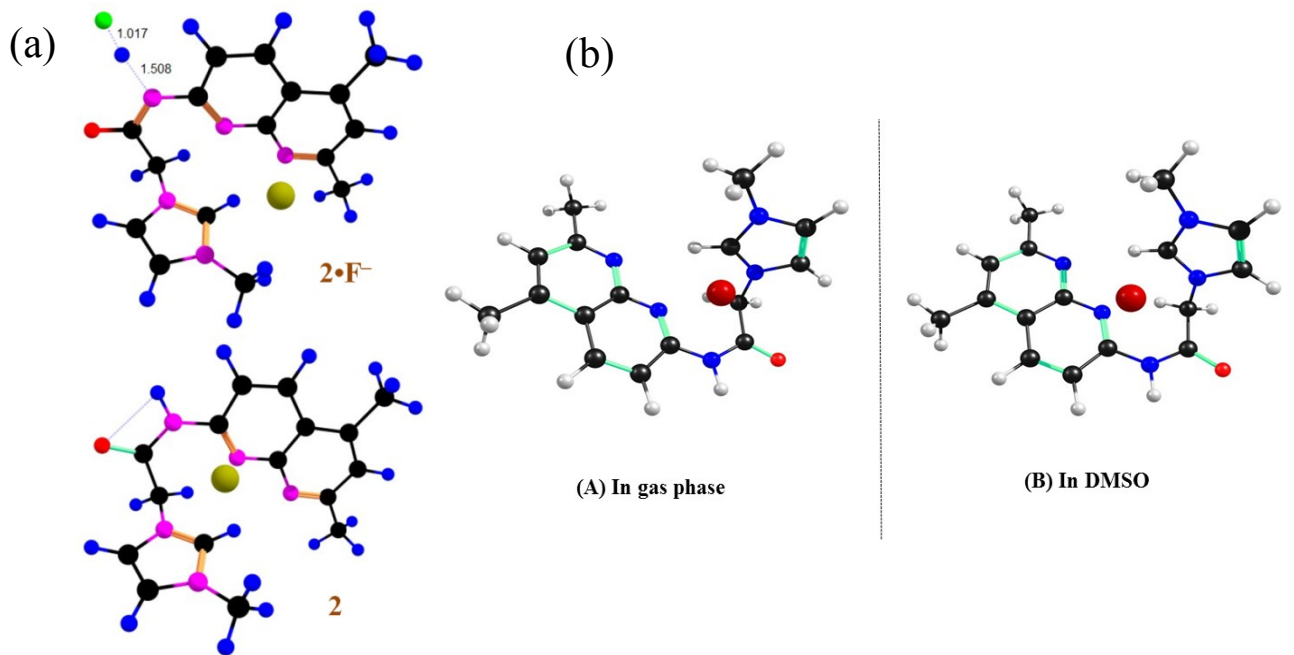


Figure S45. (a) DFT-optimized structures of **2** along with its fluoride complex in Gas phase calculated at B3LYP/6-31+G(d,p) level of theory. (b) DFT optimized structures of **2** in (A) gas phase and in (B) DMSO.

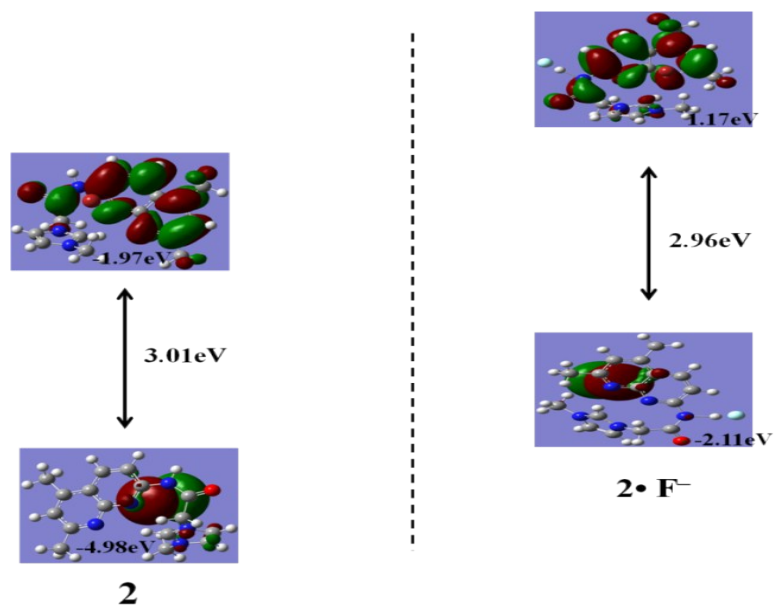


Figure S46. HOMO-LUMO energy gaps for **2** and **2•F⁻** complex.

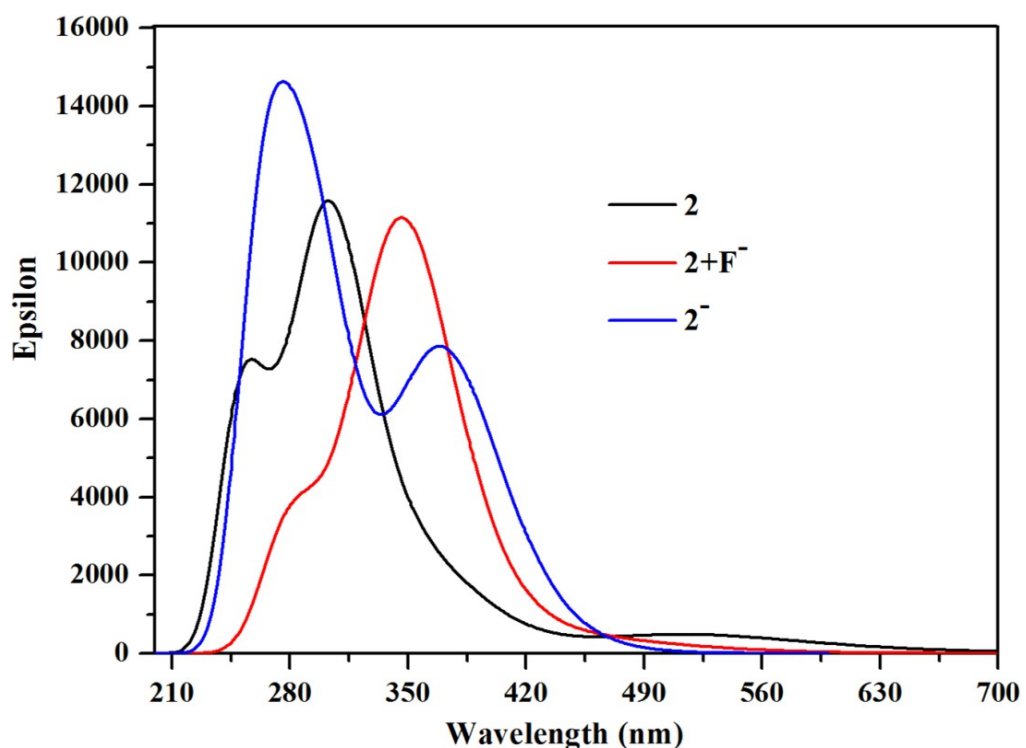


Figure S47. Absorption spectra of **2**, **2⁻**, and (**2•F⁻**) calculated by TD-DFT calculations.

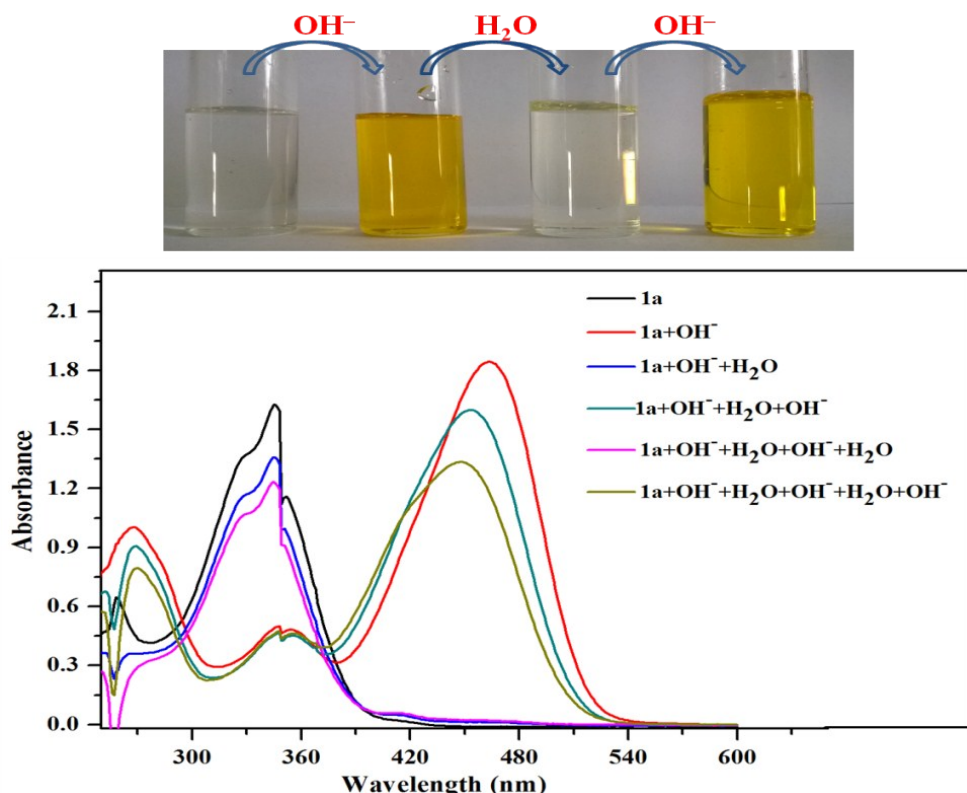


Figure S48. Colorimetric response of **1a** for reversibility and reusability tests with OH^- ions (top) and their corresponding UV-Vis spectral changes in DMSO at 298 K (bottom).

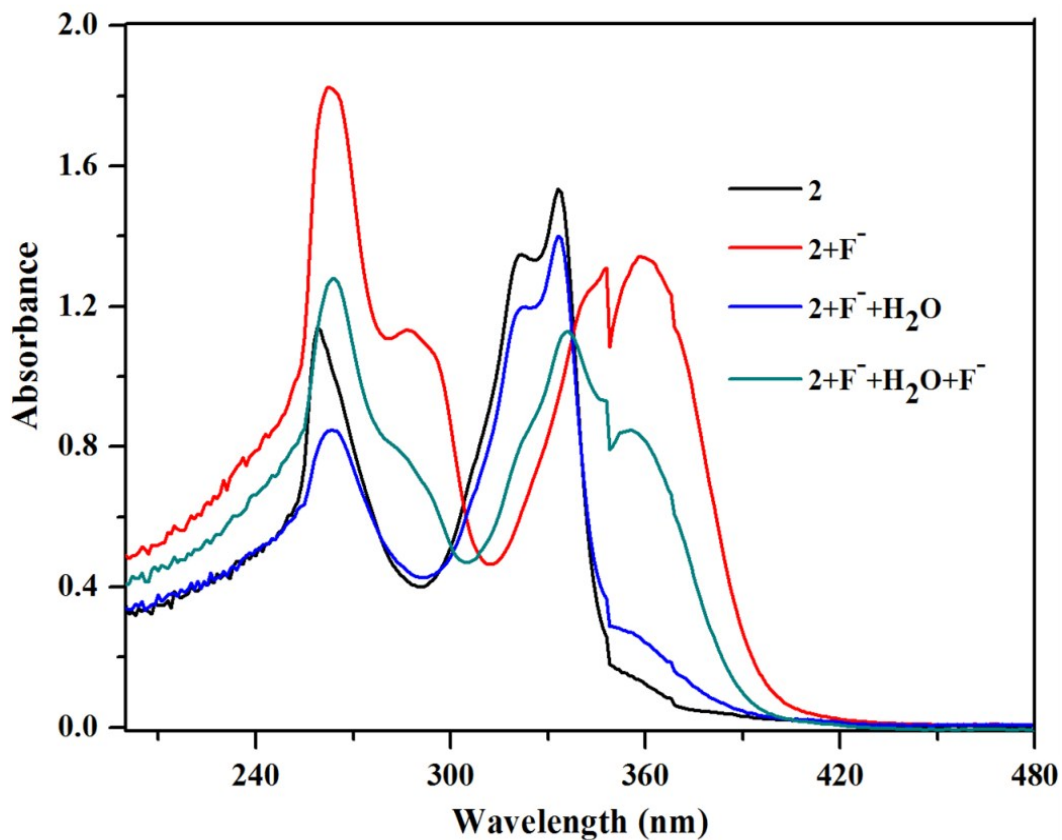


Figure S49. UV-Vis spectral response of **2** for reversibility and reusability tests with F^- ions in DMSO at 298 K.

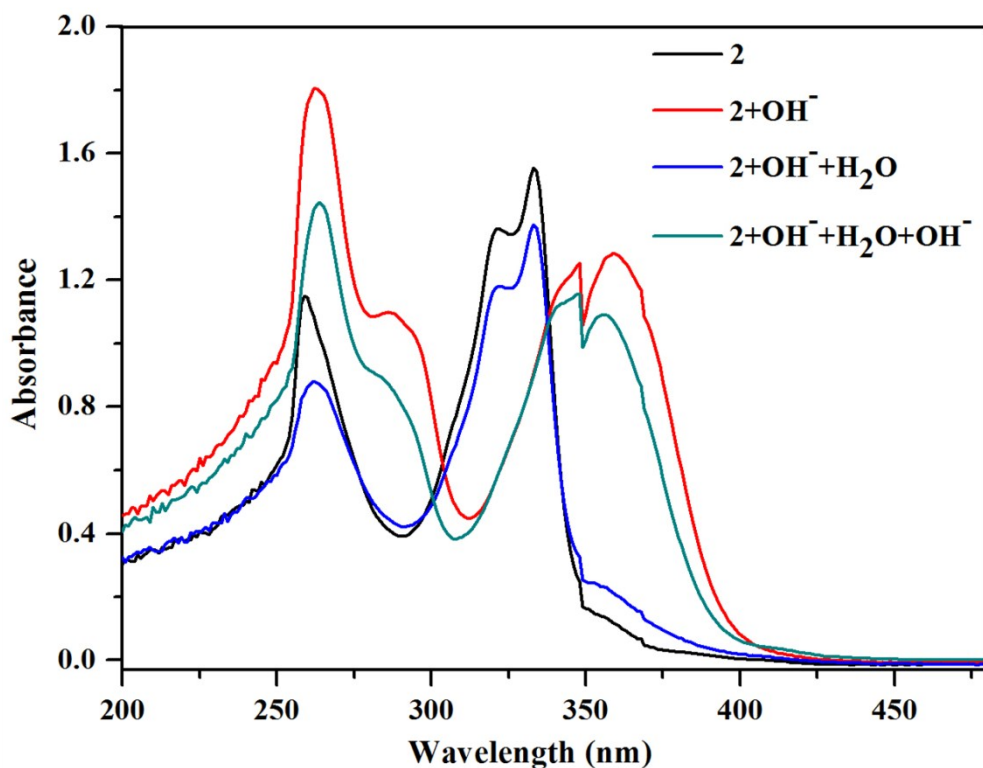


Figure S50. UV-Vis spectral response of **2** for reversibility and reusability tests with OH^- ions in DMSO at 298 K.

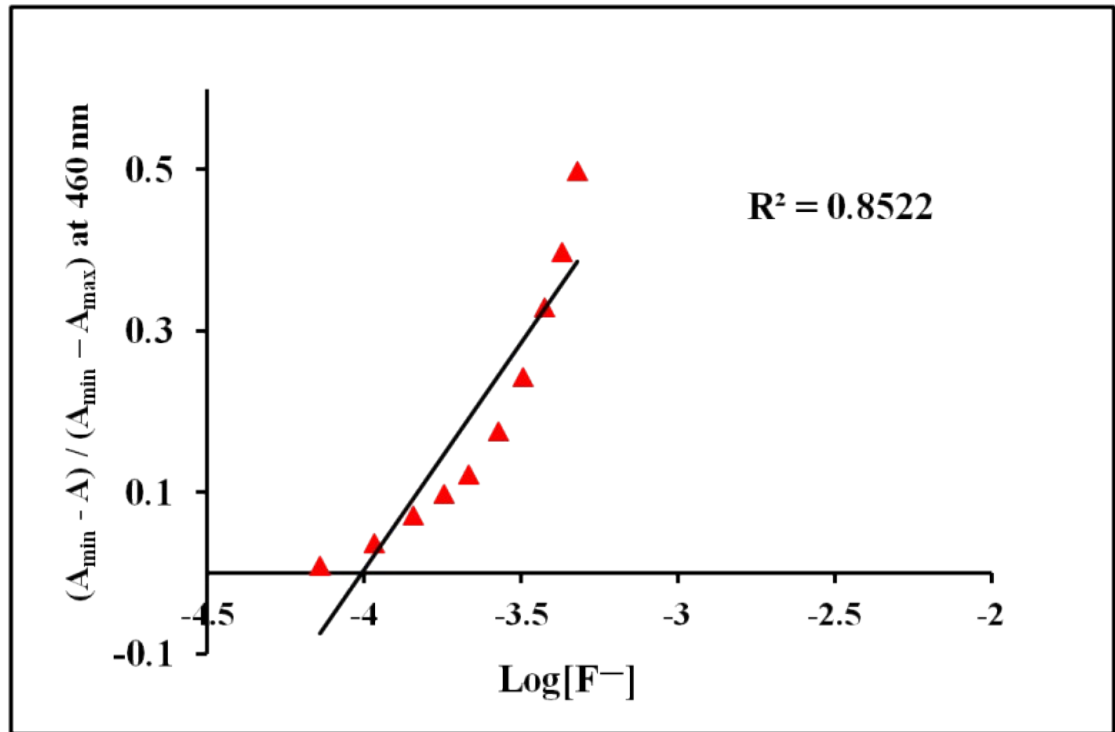


Figure S51. Absorbance of **1a** in DMSO, normalized between the minimum absorbance found at zero equiv of F^- and the maximum absorbance found at 13 eq. of F^- .

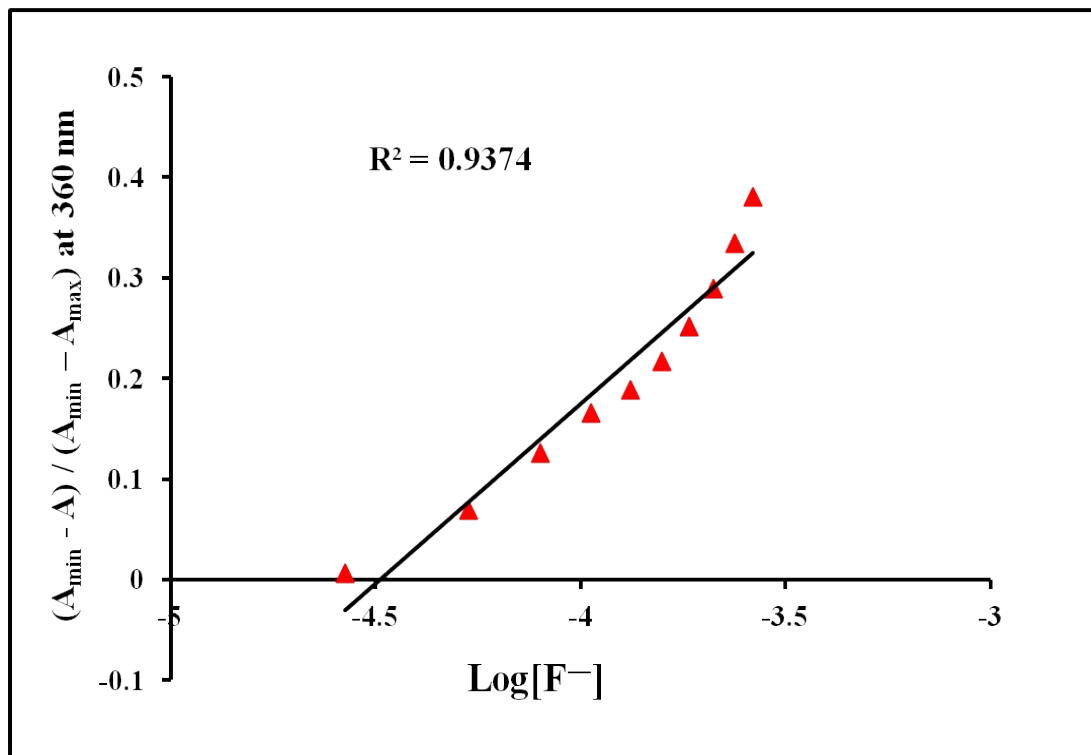


Figure S52. Absorbance of **2** in DMSO, normalized between the minimum absorbance found at zero equiv of F^- and the maximum absorbance at 3 eq. of F^- .

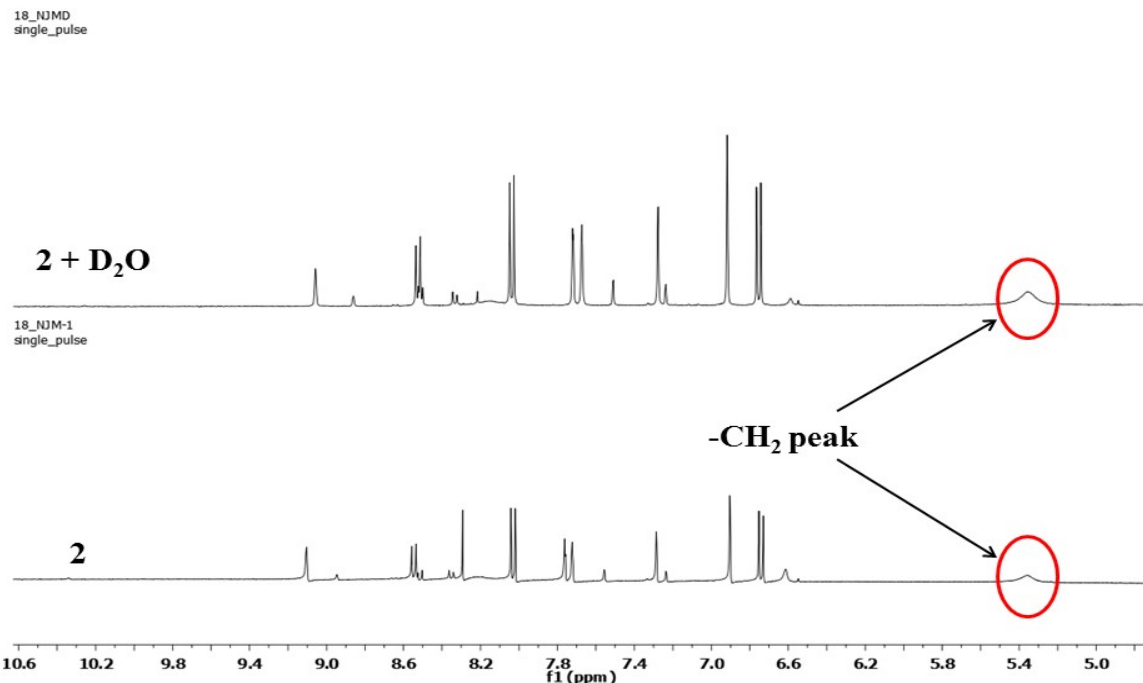


Figure S53. H/D exchange confirmed that –CH₂ protons are less acidic as the peak at 5.37 ppm did not disappear on adding D₂O in case of **2**.

Table S1: Energy of optimized molecules in DMSO and gaseous phases.

Molecule	Energy in DMSO (a.u.)	Energy in gas phase (a.u.)
1a	-1156.3318	-1156.3067
1a•F ⁻	-1256.3553	-1256.2733
2	-3541.4029	-3541.3608

Table S2: Cartesian coordinates for **1a** in DMSO

6	-6.152709000	-1.287030000	0.002131000
6	-3.955065000	-0.582741000	0.000338000
6	-4.338995000	0.793478000	-0.000730000
6	-5.732707000	1.113277000	-0.000272000

6	-6.619476000	0.057639000	0.001166000
6	-3.296783000	1.754505000	-0.002214000
1	-7.689652000	0.242668000	0.001568000
6	-1.978672000	1.362561000	-0.002505000
6	-1.707963000	-0.033171000	-0.001273000
1	-3.534130000	2.813149000	-0.003160000
1	-1.168060000	2.075388000	-0.003581000
7	-0.411882000	-0.569277000	-0.001608000
7	-2.650579000	-0.963472000	0.000035000
7	-4.864580000	-1.599878000	0.001736000
7	1.878591000	-0.783876000	-0.002018000
6	3.240483000	-0.481529000	-0.001188000
6	4.133412000	-1.576896000	-0.003702000
6	3.757905000	0.830767000	0.002124000
6	5.502848000	-1.376161000	-0.002937000
1	3.744152000	-2.590427000	-0.006265000
6	5.132448000	1.031284000	0.002909000
1	3.085274000	1.674779000	0.004017000
6	5.998150000	-0.066423000	0.000396000
1	6.184300000	-2.217132000	-0.004887000
1	5.534885000	2.036375000	0.005463000
7	7.431464000	0.152871000	0.001195000
8	7.853260000	1.318440000	0.004235000
8	8.181092000	-0.834550000	-0.001023000
6	-6.210159000	2.542127000	-0.001329000
1	-5.847446000	3.083199000	0.879793000
1	-5.848706000	3.081449000	-0.884041000
1	-7.301424000	2.585262000	-0.000593000
1	1.667851000	-1.773620000	-0.004047000
6	0.800828000	0.093219000	-0.000965000
1	-0.421757000	-1.582832000	-0.001288000
8	0.919269000	1.316140000	0.000187000
6	-7.149919000	-2.417117000	0.003647000

1	-7.799765000	-2.362614000	-0.877354000
1	-7.799439000	-2.360572000	0.884754000
1	-6.634979000	-3.379306000	0.004645000

Table S3: Cartesian coordinates for **1a** in gas phase.

6	-6.146515000	-1.287192000	0.002573000
6	-3.956047000	-0.578903000	0.000525000
6	-4.341564000	0.799096000	-0.000813000
6	-5.735648000	1.114352000	-0.000372000
6	-6.619313000	0.057452000	0.001334000
6	-3.301914000	1.762907000	-0.002511000
1	-7.690466000	0.240875000	0.001743000
6	-1.982236000	1.376174000	-0.002846000
6	-1.716579000	-0.020266000	-0.001415000
1	-3.543349000	2.821153000	-0.003584000
1	-1.168218000	2.086346000	-0.003999000
7	-0.418388000	-0.560258000	-0.001989000
7	-2.651269000	-0.952910000	0.000163000
7	-4.861611000	-1.596224000	0.002168000
7	1.873998000	-0.784324000	-0.002682000
6	3.242635000	-0.484744000	-0.001536000
6	4.133186000	-1.578557000	-0.004586000
6	3.757861000	0.825762000	0.002630000
6	5.505277000	-1.379299000	-0.003476000
1	3.743645000	-2.593436000	-0.007844000
6	5.134969000	1.023577000	0.003755000
1	3.081513000	1.667622000	0.004833000
6	5.997947000	-0.072512000	0.000733000
1	6.194366000	-2.214614000	-0.005813000
1	5.545989000	2.025670000	0.006964000
7	7.444930000	0.146841000	0.001925000
8	7.853062000	1.311285000	0.005533000
8	8.178633000	-0.846327000	-0.000737000

6	-6.216770000	2.543365000	-0.001747000
1	-5.857955000	3.087239000	0.879729000
1	-5.859351000	3.085034000	-0.885150000
1	-7.308593000	2.585315000	-0.000939000
1	1.660051000	-1.772023000	-0.005518000
6	0.796892000	0.100554000	-0.001392000
1	-0.448009000	-1.573023000	-0.000836000
8	0.919718000	1.318019000	-0.000054000
6	-7.135624000	-2.425673000	0.004331000
1	-7.785274000	-2.381393000	-0.877966000
1	-7.785058000	-2.378910000	0.886654000
1	-6.603554000	-3.378096000	0.005568000

Table S4: Cartesian coordinates for **1a•F⁻** in DMSO.

6	-6.134846000	-1.278558000	0.001632000
6	-3.938727000	-0.559064000	0.000517000
6	-4.335916000	0.813789000	-0.000242000
6	-5.730634000	1.123047000	-0.000071000
6	-6.611906000	0.061648000	0.000845000
6	-3.299153000	1.782549000	-0.001138000
1	-7.683338000	0.239785000	0.000983000
6	-1.980537000	1.398315000	-0.001225000
6	-1.688804000	0.001548000	-0.000458000
1	-3.544319000	2.839681000	-0.001754000
1	-1.173737000	2.115945000	-0.001827000
7	-0.395351000	-0.508251000	-0.000271000
7	-2.633392000	-0.933572000	0.000426000
7	-4.844324000	-1.581971000	0.001447000
7	1.865537000	-0.716861000	-0.000214000
6	3.215288000	-0.433607000	-0.000161000
6	4.097845000	-1.545174000	-0.000686000
6	3.766262000	0.871597000	0.000491000
6	5.468267000	-1.368667000	-0.000553000

1	3.684248000	-2.548397000	-0.001199000
6	5.141802000	1.047199000	0.000618000
1	3.107380000	1.727035000	0.000877000
6	5.992178000	-0.066361000	0.000101000
1	6.135298000	-2.221452000	-0.000969000
1	5.563085000	2.044839000	0.001141000
7	7.420410000	0.126076000	0.000234000
8	7.868760000	1.285370000	0.000804000
8	8.158041000	-0.874469000	-0.000188000
6	-6.218506000	2.548847000	-0.000873000
1	-5.859950000	3.092639000	0.880324000
1	-5.860732000	3.091345000	-0.883188000
1	-7.310179000	2.584366000	-0.000417000
1	1.561382000	-1.732174000	-0.000122000
6	0.806543000	0.178166000	-0.000370000
1	-0.308037000	-1.543078000	-0.000183000
8	0.919651000	1.408315000	-0.000548000
6	-7.123681000	-2.417070000	0.002471000
1	-7.773999000	-2.368140000	-0.878559000
1	-7.773729000	-2.367042000	0.883635000
1	-6.600946000	-3.375209000	0.002982000
9	0.651294000	-2.987258000	-0.000160000

Table S5: Cartesian coordinates for **1a•F⁻** in gas phase.

6	-6.168645000	-1.234286000	0.000522000
6	-3.953781000	-0.574628000	0.000253000
6	-4.322958000	0.810592000	0.000182000
6	-5.704990000	1.151007000	0.000243000
6	-6.618254000	0.114923000	0.000397000
6	-3.259864000	1.754432000	0.000047000
1	-7.685586000	0.323225000	0.000435000
6	-1.954386000	1.340215000	0.000022000
6	-1.692179000	-0.070387000	0.000125000

1	-3.479043000	2.818413000	-0.000023000
1	-1.120238000	2.027072000	-0.000095000
7	-0.416110000	-0.592102000	0.000254000
7	-2.664044000	-0.980273000	0.000242000
7	-4.891220000	-1.570351000	0.000437000
7	1.851878000	-0.808556000	0.000441000
6	3.175773000	-0.457773000	0.000080000
6	4.112936000	-1.534742000	0.000697000
6	3.701808000	0.868283000	-0.000880000
6	5.475304000	-1.312627000	0.000395000
1	3.725658000	-2.548700000	0.001385000
6	5.069740000	1.087565000	-0.001190000
1	3.013086000	1.700541000	-0.001342000
6	5.963802000	0.006090000	-0.000554000
1	6.176215000	-2.138648000	0.000864000
1	5.464889000	2.096638000	-0.001918000
7	7.381760000	0.245843000	-0.000872000
8	7.790769000	1.421935000	-0.001706000
8	8.152980000	-0.731691000	-0.000291000
6	-6.157259000	2.591312000	0.000150000
1	-5.786909000	3.127895000	0.881783000
1	-5.786964000	3.127770000	-0.881581000
1	-7.249009000	2.655609000	0.000179000
1	1.503448000	-2.135075000	0.001491000
6	0.822757000	0.087107000	0.000010000
1	-0.375780000	-1.611237000	0.000380000
8	0.881470000	1.325730000	-0.000531000
6	-7.178128000	-2.359400000	0.000700000
1	-7.827698000	-2.307769000	-0.882108000
1	-7.826772000	-2.308254000	0.884221000
1	-6.656389000	-3.318081000	0.000193000
9	1.110461000	-3.131891000	0.001115000

Table S6: Cartesian coordinates for **2** in DMSO.

7	1.125887000	-2.453748000	-0.708995000
1	1.282168000	-3.363610000	-0.287506000
7	-0.441761000	-0.725387000	-0.989262000
7	-1.854064000	1.068611000	-1.222245000
6	2.264612000	-1.963532000	-1.296875000
8	3.299330000	-2.629906000	-1.270160000
6	2.262564000	-0.603017000	-2.008655000
1	3.060585000	-0.639409000	-2.750276000
1	1.308906000	-0.393812000	-2.484010000
6	3.792734000	0.742279000	-0.494783000
6	1.682568000	1.406669000	-0.634211000
7	2.558961000	0.490890000	-1.074787000
1	4.658635000	0.136040000	-0.705239000
1	0.637975000	1.450952000	-0.905346000
6	-3.225086000	3.047003000	-1.544480000
1	-3.424046000	3.762948000	-0.738810000
1	-2.341894000	3.371957000	-2.097062000
1	-4.091891000	3.069534000	-2.214732000
6	-4.989904000	-0.895741000	1.069982000
1	-5.303967000	-1.831640000	0.594546000
1	-4.653891000	-1.143141000	2.083070000
1	-5.863547000	-0.245532000	1.150875000
6	3.638774000	1.836820000	0.301739000
1	4.346913000	2.358422000	0.924789000
7	2.320768000	2.241626000	0.188264000
6	1.679793000	3.306807000	0.965356000
1	1.391265000	2.902751000	1.938119000
1	2.383174000	4.130674000	1.083415000
1	0.798059000	3.654730000	0.428199000
35	1.037511000	-0.150474000	2.561287000

Table S7: Cartesian coordinates for **2** in gas phase.

7	1.110575000	-2.444420000	-0.774476000
1	1.308388000	-3.303935000	-0.274585000
7	-0.503063000	-0.776319000	-1.140074000
7	-1.930355000	1.001347000	-1.400651000
6	2.260315000	-1.911119000	-1.310112000
8	3.313383000	-2.535765000	-1.258427000
6	2.229774000	-0.542987000	-2.009343000
1	3.008019000	-0.573599000	-2.773561000
1	1.257500000	-0.329333000	-2.445584000
6	3.818032000	0.814804000	-0.571275000
6	1.672709000	1.371579000	-0.501658000
7	2.556130000	0.540178000	-1.077559000
1	4.680467000	0.231568000	-0.849639000
1	0.611060000	1.374737000	-0.693328000
6	-3.307494000	2.964509000	-1.755999000
1	-3.368381000	3.743272000	-0.985845000
1	-2.489767000	3.206201000	-2.437227000
1	-4.251810000	2.986436000	-2.311944000
6	-4.908572000	-0.801292000	1.207386000
1	-5.238435000	-1.779274000	0.838490000
1	-4.509028000	-0.950331000	2.217054000
1	-5.787146000	-0.156166000	1.284442000
6	3.680929000	1.873306000	0.272632000
1	4.408887000	2.388014000	0.878028000
7	2.346008000	2.240701000	0.263402000
6	1.699883000	3.145274000	1.214653000
1	1.278117000	2.521961000	2.013306000
1	2.447483000	3.838751000	1.601218000
1	0.912680000	3.706061000	0.707596000
35	0.945453000	-0.160048000	2.031170000

References

- [1] M. J. Frisch, G. W. Trucks, H. B. Schlegel, G. E. Scuseria,M. A. Robb, J. R. Cheeseman, G. Scalmani, V. Barone,B. Mennucci, G. A. Petersson, H. Nakatsuji, M. Caricato,X. Li, H. P. Hratchian, A. F. Izmaylov, J. Bloino, G. Zheng,J. L. Sonnenberg, M. Hada, M. Ehara, K. Toyota,R. Fukuda, J. Hasegawa, M. Ishida, T. Nakajima, Y. Honda,O. Kitao, H. Nakai, T. Vreven, J. A. Montgomery Jr,J. E. Peralta, F. Ogliaro, M. Bearpark, J. J. Heyd,E. Brothers, K. N. Kudin, V. N. Staroverov, R. Kobayashi,J. Normand, K. Raghavachari, A. Rendell, J. C. Burant,S. S. Iyengar, J. Tomasi, M. Cossi, N. Rega, J. M. Millam,M. Klene, J. E. Knox, J. B. Cross, V. Bakken, C. Adamo,J. Jaramillo, R. Gomperts, R. E. Stratmann, O. Yazyev,A. J. Austin, R. Cammi, C. Pomelli, J. W. Ochterski,R. L. Martin, K. Morokuma, V. G. Zakrzewski, G. A. Voth,P. Salvador, J. J. Dannenberg, S. Dapprich, A. D. Daniels,O. Farkas, J. B. Foresman, J. V. Ortiz, J. Cioslowski, and D. J. Fox, Gaussian 09, Revision A.02, Gaussian, Inc.,Wallingford CT, 2009.
- [2] D. D. Censo, S. Fantacci, F. D. Angelis, C. Klein,N. Evans, K. Kalyanasundaram, H. J. Bolink, M. Graltzel, M. K. Nazeeruddin, Synthesis, Characterization, and DFT/TD-DFT Calculations of Highly Phosphorescent Blue Light-Emitting Anionic Iridium Complexes, Inorg. Chem. 47 (2008) 980-989.
- [3] K. Wolinski, J. F. Hilton, P. Pulay, Efficient implementation of the gauge-independent atomic orbital method for NMR chemical shift calculations, J. Am. Chem. Soc. 112 (1990) 8251-8260.
- [4] A. Frish, M. J. Frisch, Gaussian 98 User's Reference; Gaussian,Inc. Pittsburgh, PA., 1998.